Journal of Nuclear Materials 578 (2023) 154340

Contents lists available at ScienceDirect

Journal of Nuclear Materials

journal homepage: www.elsevier.com/locate/jnucmat

Comparative study of fission product release of homogeneous and heterogeneous high-burn up MOX fuel by Knudsen Effusion Mass Spectrometry supported by EPMA, SEM/TEM and thermal diffusivity investigations

Jean-Yves Colle[a,*], Thierry Wiss[a], Oliver Dieste[a], Philipp Pöml[a], Dragos Staicu[a], Terje Tverberg[b], Stéphane Bremier[a], Rudy J.M. Konings[a], Vincenzo V. Rondinella[a], Takeshi Sonoda[c], Akihiro Sasahara[c], Shoichi Kitajima[c]

[a] European Commission, Joint Research Centre, Karlsruhe, P.O. Box 2340, Karlsruhe D-76125, Germany
[b] Institute for Energy Technology, P.O. Box 173, Halden NO-1751, Norway
[c] Central Research Institute of Electric Power Industry (CRIEPI), 2-6-1, Nagasaka, Yokosuka-shi, Kanagawa 240-0196, Japan

ARTICLE INFO

Article history:
Received 11 April 2022
Revised 10 February 2023
Accepted 13 February 2023
Available online 16 February 2023

Keywords:
Nuclear fuel
Fission product release
Knudsen effusion mass spectrometry
Mixed oxide fuel
Homogeneous
Thermal diffusivity

ABSTRACT

The fission product release of two irradiated mixed oxide (MOX) fuel variants from the high burn-up disk irradiation test IFA-655 in the Halden reactor was investigated by Knudsen Effusion Mass Spectrometry (KEMS). The fresh samples were provided and characterised within the NFIR[1] program. Both fresh fuel variants contained 16 wt.% plutonium but differed principally by the distribution of the plutonium: in one it was heterogeneously dispersed, in the other one homogeneously. The fission products release (Kr, Xe, I, Cs, Te, Sr, Nd) measured by KEMS as a function of annealing temperature is reported. The gas release (including helium) has been measured quantitatively. The interpretation of the release measurements is supported by microstructure and elemental analyses (SEM, TEM, EPMA). A correlation has been made with results from thermal diffusivity measurements obtained on the same fuels.

1. Introduction

The overall behaviour of MOX (Mixed OXide) fuel in LWRs (Light Water Reactor) is very similar to that of UO_2 fuel when operated in similar conditions. This has been demonstrated by dedicated research programs conducted worldwide and in surveillance programs in several countries. They have also revealed specific aspects of in–pile behaviour of MOX fuel. When comparing MOX and UO_2 fuels, it is necessary to take into account the differences in distribution of the fissile isotopes [1]. For technological reasons, the industrial MOX fuel production is based on a dry powder mixing process, which does not lead to a fully homogeneous product. Industrial MOX pellets from the so-called MIMAS (MIcronized MASter blend) process are heterogeneous [1–3], have a microstructure with plutonium-rich islands in a uranium oxide matrix, which has a low Pu concentration. The MIMAS fabrication consists of a two-step mixing process in which first a 30% Pu-rich master blend is produced by micronisation, which is subsequently mixed with UO_2. As a result, the maximum Pu-concentration in the Pu-rich islands is around that value since the Pu and U lattice diffusion does not lead to full homogeneity during the sintering process at 1600–1700 °C. The OCOM (Optimized CO-Milling) method has a similar approach [4]. An alternative fabrication method was developed by British Nuclear Fuels Limited (BNFL) in the United Kingdom, and is based on attrition milling, the so–called Short Binderless Route (SBR). In this process, UO_2 and PuO_2 are mixed and milled in several stages in an attrition mill to obtain a homogeneous powder that, after compacting and sintering, yields a more homogeneous microstructure with very few plutonium–rich spots [5].

The burnup of MIMAS MOX fuel is inhomogeneous as well, and the Pu-rich islands and spots have a much higher local burnup than the surrounding matrix. This leads to differences in structural evolution compared to UO_2 fuel, such as the development of high burn-up structure (HBS) inside the islands, which in turn can lead to different fission gas behaviour and release. Such differences have been reported in literature previously [6], but it is not fully clear whether these can be attributed to the microstructure only,

* Corresponding author.
E-mail address: jean-yves.colle@ec.europa.eu (J.-Y. Colle).
[1] NFIR: https://www.epri.com/portfolio/programs/108031

https://doi.org/10.1016/j.jnucmat.2023.154340

Table 1
Fresh fuel characteristics and irradiation data of the two MOX fuel variants.

Fuel name	MOX1	MOX2
IFA-655 number	rod11	rod12
Fuel type	MOX homogeneous	MOX heterogeneous
Fabrication	sol-gel	direct powder mixing
Grain size (μm)	10–15	UO_2 ~ 10
Agglomerate size (μm)		32<PuO_2<63
Pu vector (%): 238, 239, 240, 241, 242, (Am/Pu in August 2000)	0.068, 85.77, 13.29, 0.59 0.29, (1.23)	0.059, 85.85, 13.25, 0.57 0.27,(1.22)
U enrichment (wt%)	^{235}U/U: 0.31	^{235}U/U: 0.27
U vector (%): 234, 235, 236, 238	0.0046, 0.33, 0.025, 99.64	0.036, 0.26, 0.007, 99.73
Pu content (wt%HM)	16	16
Density (%TD)	96.0	96.0
O/M	1.986	1.998
Target Irradiation temperature (°C)	700 (973 K)	700 (973 K)[1]
Estimated Temperature at discharge (°C)	590 (863 K)	600 (873 K)
Burnup (MWd/kgHM)	116	118
Discharge power (kW.m^{-1})	50.4	51.7
FGR (%)[2]	17	47[3,4]
FGR (%)from puncture data (not accounting for He release)[5]	25	60
KEMS samples weight (mg)	MOX1 - 16.8 (1 pcs)	MOX2 - 8.6 (1 pcs)
KEMS temperature ramp (K/min)	10	10
Date of KEMS measurement	December 2014	March 2012

[1] 1 day 800–900 °C after Dec 2002.
[2] Fractional Gas Release during irradiation in% calculated from in-pile pressure data for sibling rodlets (rodlets 5 and 6) in the lower cluster in IFA-655.
[3] 33% if burst not accounted.
[4] results for sibling rodlet in the lower cluster in IFA-655 with the same fuel.
[5] puncture data for sibling rodlets in the lower cluster in IFA-655 with the same fuel.

or whether inherent differences in irradiation conditions (e.g. heat rate evolution) also contribute to fission gas release.

To have a better understanding of the microstructure influence on fission gas release, two MOX fuels are investigated, a homogeneous material obtained by an aqueous gel-supported precipitation process and a heterogeneous material obtained by blending of PuO_2 and UO_2 powders.[2] The fuels were irradiated in the Halden Reactor as part of the IFA-655 irradiation [7]. In the current paper, we report the results of extended post-irradiation examinations (PIE) that will help to determine whether the MOX microstructure affects the fission gas behaviour at high burnup.

2. Materials and techniques

2.1. Fuel synthesis

The two fresh MOX fuels had a Pu content of 16 wt% Heavy Metal (HM), 86% of which was fissile. They differ only by the distribution of the plutonium. Relevant data of the samples studied are shown in Table 1.

The MOX1 fuel was obtained from (U,Pu)O_2 powder synthesised by the sol-gel method [8–10]. PuO_2 was dissolved in nitric acid, followed by denitration and a uranium solution was prepared by dissolving uranyl nitrate. These solutions were then mixed in the required ratio, and the chemical composition was measured. Next, the feed solution together with additives was drop-wise dispersed and collected in an ammonia gelation bath, followed by conversion into solid particles, which were subsequently washed and dried. The particles were pre-calcined (400 °C) and calcined (800 °C) and the resulting powder pressed into pellets. To prepare the MOX2 fuel, PuO_2 and UO_2 powders were mixed using a mechanical blender and subsequently pressed. Final pellets were sintered for 4 h at 1700 °C in Ar for the MOX1 and 6 h at 1700 °C in Ar/6%H_2 with 1050 ppm H_2O for the MOX2. The disks were prepared by cutting the pellets.

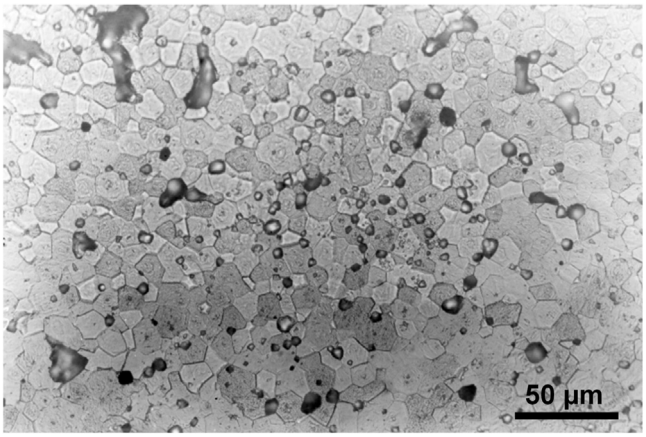

Fig. 1. Ceramographic micrograph after Pu-etching of the MOX1 pellet before irradiation highlighting a homogeneous distribution of both types of cations.

Figs. 1–3 show ceramographic micrographs of the fresh MOX1 and MOX2 fuels. Note that in Fig. 1 some grain pull out during sample preparation (black areas) as well as some porosity (black with white reflections) can be observed. The plutonium-rich areas of MOX2 can be seen in the Ceramographic micrograph in Figs. 2 and 3. In the MOX1 sample the plutonium is homogeneously distributed in the fuel matrix forming a single (U,Pu)O_2 phase, as a result of the aqueous synthesis route. In the MOX2 the plutonium is concentrated in PuO_2-rich islands (Fig. 2) of a

[2] The fuels were part of a batch of fresh fuels prepared and characterised at JRC Karlsruhe in the framework of the NFIR program.

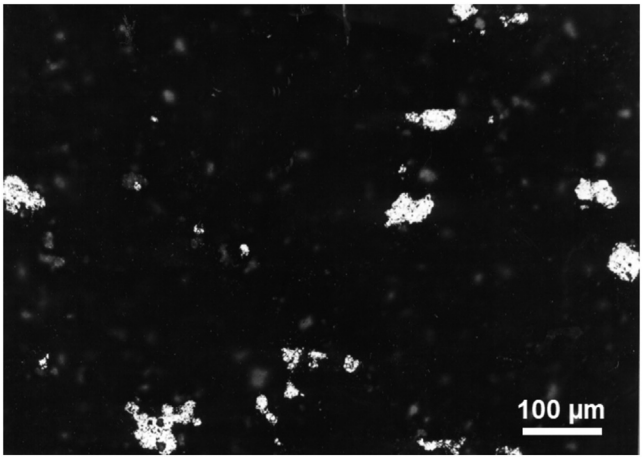

Fig. 2. Ceramographic micrograph the MOX2 pellet before irradiation (Pu etched: rich Pu areas in bright).

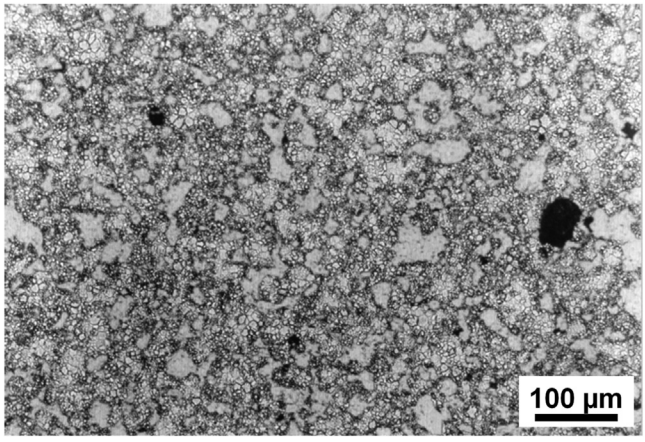

Fig. 3. Ceramographic micrograph of the MOX2 pellet before irradiation (U-etching, light grey areas are U).

few tens of µm in diameter in the UO_2 matrix, therefore forming a heterogeneous two phase fuel as is demonstrated by the plutonium line scans measured by Electron Probe Micro Analysis (EPMA) (Fig. 4).

Both fuels were synthetized at the European Commission - Joint Research Centre Karlsruhe (EC-JRC KA) in 2000. They were shipped to Norway for irradiation in the Halden Boiling Heavy Water Reactor (HBWR) For the irradiation they were cut into disks of 8.2 mm diameter and 1 mm thickness separated by a thick (3 mm) molybdenum disk in order to have a homogenous irradiation temperature and reach a flat burnup profile due to the high enrichment [11–13].

2.2. Irradiation in the Halden reactor

The disks were irradiated in the IFA-655 experiment in the HBWR commencing in August 2001 and ending in October 2006. This experiment had as objective the study of properties of the High Burnup Structure (HBS) in UO_2 and in MOX fuels. The experiment was divided into two phases: a steady base irradiation period (up to 120–130 MWd/kgHM) to obtain high burn-up fuel having the HBS and, for a selection of rodlets, a fast power transient sequence to study fuel elongation and rodlet internal pressure.

The test rig used for the irradiation IFA-655 contained 12 short rodlets in two separate axial clusters. Each cluster had four UO_2 and two MOX rodlets. The four UO_2 rodlets in a given cluster were of either standard (~9 μm) or large (~30 μm) grain size, while

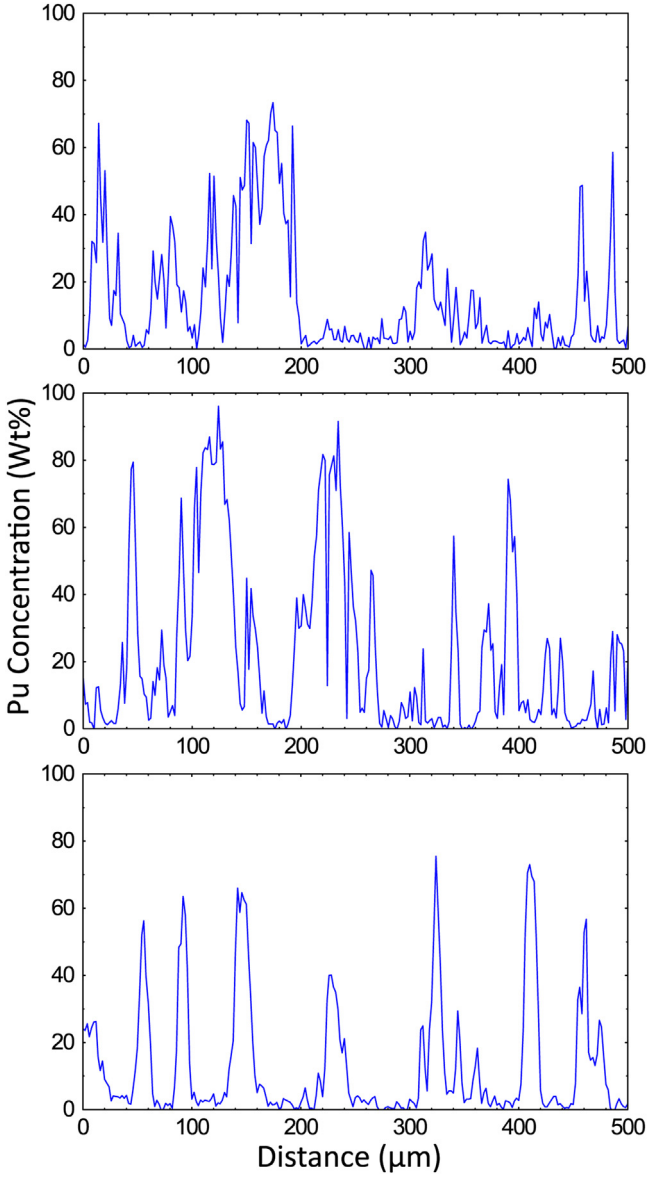

Fig. 4. EPMA line scans of the plutonium concentration across the fresh MOX2 pellet at three positions.

the two MOX rodlets in the same cluster had one rodlet of homogeneous MOX1 and the other heterogeneous MOX2. The rig was operated under typical HBWR conditions, i.e. boiling heavy water at 34 bar (235 °C). The upper cluster of rodlets (rodlets 7 to 12) had gas lines to provide a means of monitoring fission gas release, and fuel thermocouples to monitor the temperature in-pile. The Halden-type gas-flow rig was used to evaluate the release rate during irradiation of fuel rodlets. From release-to-birth rate (R/B ratio) measured in the gas-flow rig information about parameters of fission gas release, such as diffusion coefficient, surface-to-volume ratio (S/V) can be extracted [14]. The lower cluster of rodlets (rodlets 1 to 6) was designed on the basis of being subjected to a transient after the end of the base irradiation in the IFA-655 rig. The rodlets were all sealed, and equipped with pressure transducers and fuel extensometers for online monitoring of pressure and fuel elongation. In the end, after the IFA-655 irradiation was completed, transient testing was performed on four of the six lower cluster rodlets, in a separate rig.

Common for all twelve rodlets was that they contained 25 fuel disks of thickness ~1 mm, sandwiched between Mo disks and con-

strained by Mo rings. The role of the Mo disks was to ensure a uniform and low radial temperature profile. The length of the disk column was nominally 100 mm (including Mo- and fuel disks). For the rodlets 11 (MOX1) and 12 (MOX2) of this study, the gap between the Mo disk and cladding was 250 μm, as required to reach the targeted irradiation temperature of 700 °C (a small radial temperature gradient was expected as the fuel was placed between two molybdenum disks). Details on the temperature measurement and assessment and power history can be found for the upper rodlets cluster in [13]. As mentioned above, these two upper cluster rodlets were instrumented with gas lines to provide a means of monitoring fission gas release, and fuel thermocouples to monitor the temperature in-pile. Due to the intermittent gas flushing of these rodlets by means of the gas flow system, there was no means to estimate the cumulative fission gas release of these rodlets for the full IFA-655 irradiation. However, for the sibling rodlets (rodlets 5 and 6) in the lower cluster, the rodlet pressure increase from gas release was monitored with the pressure transducer. The data from the lower cluster rodlets are presented in [13]. From this reference, it can be deduced that the power histories for all four MOX rodlets were very similar, regardless of cluster position (upper vs. lower).

As the two MOX rodlets from this study (11 & 12) were positioned in the same upper cluster, the burnup is very similar. During irradiation, the fuel temperature and open fuel porosity were measured in the corresponding rodlets in the upper cluster. Open fuel porosity or surface-to-volume ratio (S/V) was estimated by monitoring the release of radioactive fission gas using gamma spectrometry. Several measurements of short-lived fission gases have been performed during each cycle at burnup increments of approximately 5 MWd/kgHM [15]. Only rodlet 12 (MOX2) showed significant rise in elongation and open porosity, quantified by the Surface-to-Volume ratio (S/V), and release-to-birth rate (R/B) values [14,16,17]. This is likely connected to the increase in fuel temperature, and associated fission gas release, which occurred by mal-operation for this fuel after the reactor restart in late December 2002 at a burnup ~40 MWd/kgHM [7,13,18]. The fuel operated for 24 h between 800 and 900 °C and the measured temperature actually went above 1000 °C for a very short period. The reactor cycle that ended the IFA-655 irradiation was terminated with a reactor scram, in order to preserve the microstructure of the fuel at the end of the irradiation.

The fuels were unloaded after irradiation in October 2006 and four disk samples were transported back to EC-JRC KA.

2.3. Characterization

The release behaviour of the fission products (FP) as well as the vaporisation behaviour of the actinide compounds forming the matrix were measured by the KEMS technique [19,20]. A tungsten Knudsen cell with an internal height of 12 mm and an internal diameter of 7 mm was used. The effusion aperture had a diameter of 0.5 mm and a length of less than 0.2 mm. The mass spectrometric measurement were done with a Pfeiffer Vacuum QMA 400 quadrupole mass spectrometer (QMS). The QMS is equipped with a cross beam electron bombardment ion source. For the ionisation, an electron energy of about 40 eV was chosen, avoiding excessive fragmentation while enabling enough ionisation efficiency. The signal was measured from the mass spectrometer secondary electron multiplier. The spectrum was recorded with a speed of 0.5 s/mass: at low temperatures (below ~1500 K) for the mass range 3–5 amu (Helium) and 82–140 amu (volatile FP) and at high temperature (above ~1500 K) for the mass range 3–5 amu (helium), 82–180 amu (all FP) and 230–290 amu (actinides).

Single fragments of 16.8 mg of MOX1 and 8.6 mg of MOX2 were analysed by KEMS (Table 1). The samples were heated in the Knudsen cell with a temperature ramp of 10 K.min^{-1} up to complete vaporisation of the UO_2/PuO_2 matrix at around 2600 K. During the heating, helium, fission products and actinides compounds were released or vaporised from the sample. They escaped the Knudsen cell by the effusion hole forming a molecular beam. The beam was analysed by the quadrupole mass spectrometer. To quantify the helium and fission gases present in the samples, the gas released from the KEMS was collected and measured using the Q-GAMES (Quantitative gas measurement system), which is described in detail in [21].

Additional experiments were done for the MOX1 fuel during which the heating was interrupted in order to observe the microstructure changes at different stages of the release by electron microscopy. Based on the analysis of the complete release profile of the first MOX1 sample, three temperatures of interest were chosen: 1250 K, 1520 K and 2000 K corresponding to specific features observed in the release profile i.e. burst, peak, plateau or onset for release. For this purpose additional fragments of MOX1 (a single piece per measurement) were heated in the KEMS up to the selected temperatures and subsequently analysed by Scanning Electron Microscopy (SEM) and Transmission Electron Microscopy (TEM).

The SEM used in this study was a nuclearized Philips^{TM} XL40 [22] equipped with secondary and backscattered electron detectors (SE and BSE). The TEM was a FEI^{TM} Tecnai G2 equipped with a field emission gun (FEG) and a high angular annular dark field detector (HAADF in Scanning mode, STEM). The TEM samples were prepared by crushing a small fuel fragment in methanol using an agate mortar. The resulting suspension was dropped on a copper carbon coated TEM grid [22]. Because the MOX1 material was homogenous, electron microscopy of selected areas was considered representative of the full sample.

The EPMA measurement was performed on a CAMECA SX100R microprobe, which is fully shielded for the analysis of irradiated fuel samples. It is equipped with four vertical spectrometers, two of which have quartz $10\bar{1}1$ crystals for the analysis of actinide elements. Analyses were performed at 25 keV acceleration potential and 250 nA beam current. The quantitative maps were acquired on a 100 × 100 µm area with 310 × 310 pixels using a pixel dwelling time of 150 ms. As reference materials UO_2, PuO_2, Pollucite ($(Cs,Na)_2Al_2Si_4O_{12}\cdot H_2O$), NdF_3, Mo, and Ru were used. For Xe, a calibration curve approach was used and its intensity related to Sb [23]. A correction was applied for the overlap of U_{M3-N4} on Pu Mβ.

Additionally, the thermal diffusivity, α, was measured in a laser-flash device (LAF) installed in a lead-shielded glove box provided with remote manipulators [24]. The sample is heated to the measurement temperature in a high frequency furnace under a nitrogen atmosphere of 10^{-2} mbar. The sample can be observed during the heating process, which makes it possible to determine its behaviour during heating, in particular to observe the onset of fragmentation. The thermal diffusivity is determined by applying a laser pulse (10 milliseconds) to the front surface of the sample and measuring the temperature response on the opposite surface. The thermal diffusivity and various heat losses are calculated from the experimental thermogram by a numerical fitting procedure.

For the current samples, the thickness variations were of the order of 3% and the resulting relative uncertainty on the measured thermal diffusivity is about 6%. The temperature was measured with an accuracy of 5 K. The thermal diffusivity was measured during thermal annealing cycles by starting at low temperature (ca. 520 K).

The thermal conductivity $\lambda(T)$ was calculated from the thermal diffusivity, $\alpha(T)$, the heat capacity, $C_p(T)$, and the density, $\rho(T)$, and was normalised to 5% porosity by using the equation recom-

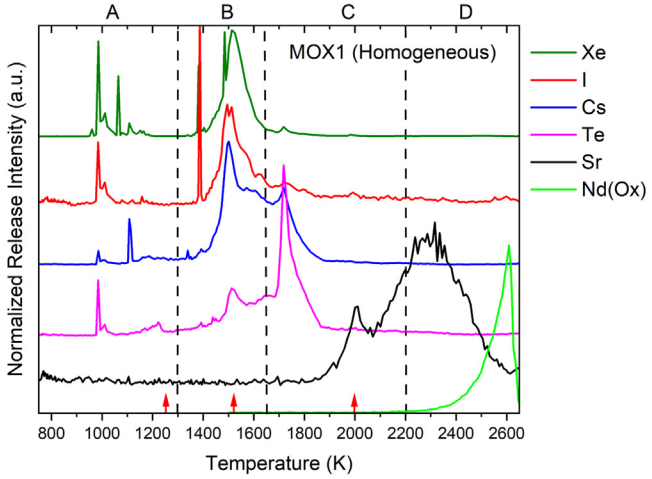

Fig. 5. Release intensity (mass spectrometer signal, linear scale) of selected fission products from the MOX1 sample as a function of the annealing temperature (the red arrows on the bottom axis are the temperatures at which SEM pictures were taken).

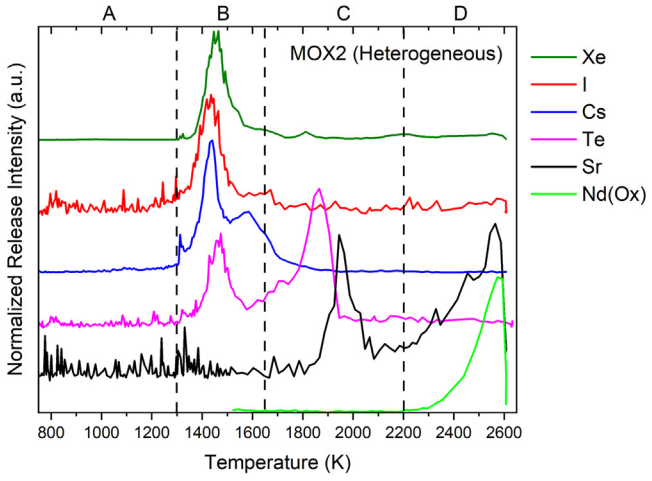

Fig. 6. Release intensity (mass spectrometer signal, linear scale) of selected fission products from the MOX2 sample as a function of the annealing temperature.

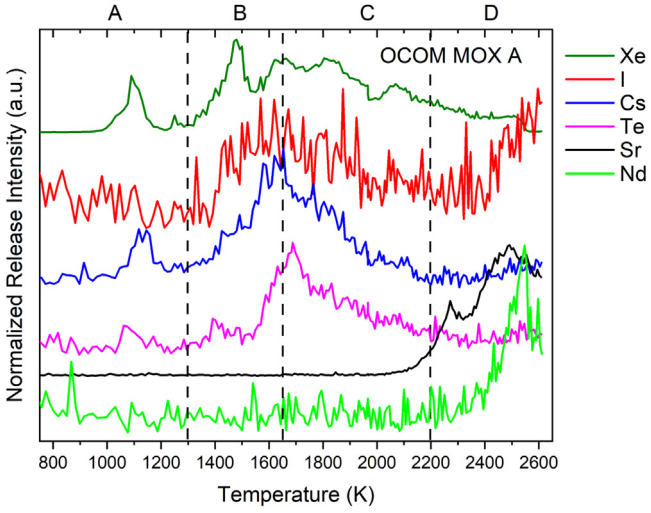

Fig. 7. Fission product release profiles (mass spectrometer signal, linear scale) of an OCOM MOX fuel partially reported in [30] (radial position 0.58 < r/r0 < 0.96).

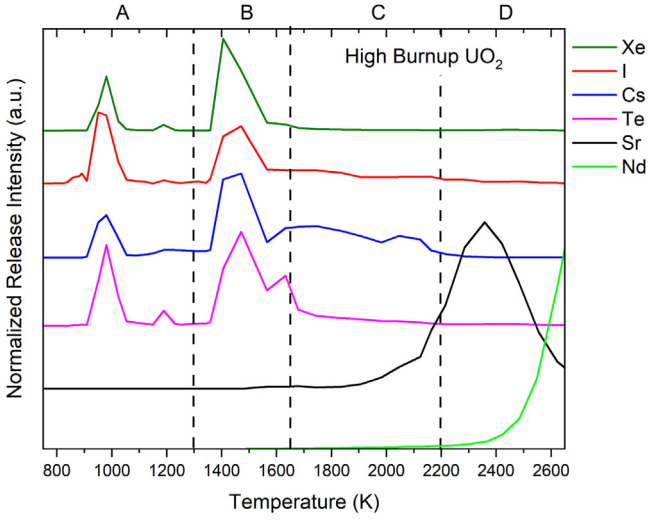

Fig. 8. Fission products release profiles (mass spectrometer signal, linear scale) of a High Burnup UO_2 fuel as reported in [37].

mended in [25]:

$$\lambda_{95}(T) = \frac{1 - 0.05f(T)}{1 - Pf(T)}\ \alpha(T)\rho(T)C_p(T) \quad (1)$$

where $f(T) = 2.6–0.5\ (T\text{-}273.15)/1000$, and P is the porosity volume fraction and T is expressed in °C. The density was deduced from the value measured at ambient temperature and the thermal expansion coefficient recommended by Fink for fresh UO_2 [25], which is also considered as valid for LWR MOX fuel.

3. Results

3.1. Release of fission products

Figs. 5 and 6 show the release profiles of a selection of key fission products (Xe, I, Cs, Te, Sr, Nd) from MOX1 and MOX2, respectively, as measured by mass spectrometry. For comparison purposes, release measurements obtained under similar conditions respectively from an OCOM MOX and a high burnup UO_2 fuel (Table 2) are shown in Figs. 7 and 8. A comparison is discussed in Section 4.3. The fission products selected cover the different chemical behaviour, volatile, semi-volatile, gaseous, metallic or precipitated [26]. Four temperature ranges have been identified in an attempt to classifying the release as a function of the possible evolution of the microstructure. For convenience, temperature ranges covering the main release feature have been designated by letters A, B, C and D. These correspond respectively to the following ranges (in K): <1300, 1300–1650, 1650–2200, >2200.

Similarities but also clear differences in terms of FP behaviour are observed between the two types of MOX:

- In interval A, the range <1300 K, the release profiles of FPs from the homogeneous MOX1 shows spikes at lower temperatures, which are not present at all in the heterogeneous material (MOX2). These spikes show a strong correlation between Xe and I, and to a lesser extent Te, while Cs release appears at a bit higher temperature, i.e. 1100 K. It should be realised that the masses were measured sequentially in the spectrometer from the light to the heavy, and thus a slight time separation occurred as a result of which some fast releases may thus have been missed in the NIR data. This may explain the difference in the release of krypton and xenon Figs. 9 and 10.
- In the temperature range 1300–1650 K (interval B) the fission gas Xe and the volatiles I, Cs and Te all show a strongly correlated release in both materials. It is the main interval for re-

Table 2
Characteristics of the fuels that are used for comparison.

Fuel name	OCOM MOX	high burnup UO_2
Fuel Type	MOX heterogeneous	UO_2
Fuel fabrication	Powder mixing	From powder
Irradiation	PWR (4 cycles)	PWR (9 cycles)
U enrichment (wt%)	^{235}U/U 0.72	^{235}U/U 3.5
Pu content (wt%HM)	5.07	
Grain size (μm)	UO_2 5–6	9–12
Agglomerate size (μm)	< 200	
Sample location	close to cladding	close to cladding
Average burnup sample (MWd/kgHM)	~ 45	~200
Burnup Pu Islands (MWd/kgHM)	~200	
Estimated irradiation temperature (°C)	581–1039	~ 450 (Close to cladding)
Linear power (kW.m^{-1})	20.4	14 (discharge)
Density (%TD)	95	95
Sample weight (mg)	4.2 (1 pcs)	6.2 (1 pcs)
KEMS temperature ramp (K/min)	10	30
Date of KEMS measurement	March 2007	June 2005

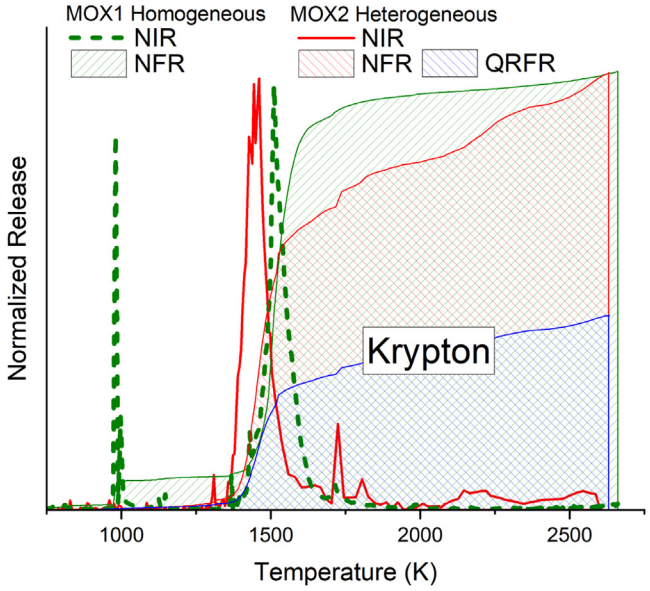

Fig. 9. Normalized Instantaneous and Fractional Release (NIR and NFR) (linear scale) of Krypton from MOX1 and MOX2 as well as Quantitative Relative Fractional Release (QRFR) of MOX2 Normalized to Kr quantities per g of fuel from MOX1 (Quantities measured by Q-Games, see Section 3.2 and Table 3).

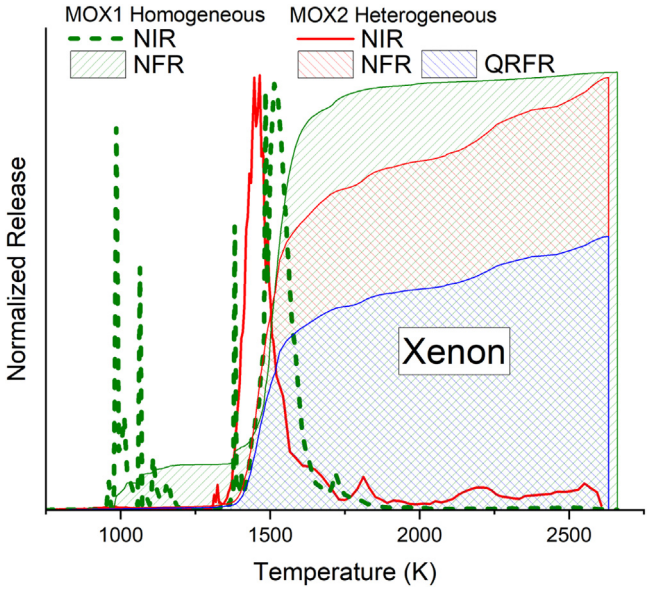

Fig. 10. Normalized Instantaneous and Fractional Release (NIR and NFR) (linear scale) of Xenon from MOX1 and MOX2 as well as Quantitative Relative Fractional Release (QRFR) of MOX2 Normalized to Xe quantities per g of fuel from MOX1 (Quantities measured by Q-Games, see Section 3.2 and Table 3).

lease for Xe and I in both MOX1 and MOX2. At higher temperatures, no significant release is observed for MOX1, while for MOX2 some more release was observed until the total vaporisation. The Cs release profile is in both cases more diffuse and is distributed in a wider temperature range, suggesting more than one release event or mechanism.

- In interval C between 1650 and 2200 K, additional release stages for Te and Cs with a substantial release are observed. However, we observe remarkable differences between the two samples:
  - In the homogeneous MOX1, the Te signal is clearly correlated with the Cs signal with a release taking place just above 1700 K. It could be speculated that some Cs_2Te has formed, possibly during the annealing at high temperature, as shown recently by Rochedy, who observed that in UO_2 implanted with Cs and Te annealed at 1373 K such Cs and Te precipitate together in bubbles sometimes with a decoration of the bubbles with Te [27].
  - In the heterogeneous MOX2, the second tellurium release occurs at significantly higher temperature (around 1900 K) and is **not** correlated to Cs release, as is the case for MOX1. This means that in MOX2 other phases/species may govern tellurium release and chemistry. Based on thermochemical calculations, Rochedy [27] suggested that phases like U_2O_2Te can form and dominate at high temperature. This phase (and possibly the analogues Pu_2O_2Te and their solid solution) could have formed in the very high burnup Pu-rich inclusions at higher oxygen potential.
- The release of Sr takes place in intervals C and D (> 2000 K). The homogeneous MOX1 shows two peaks that are strongly overlapping: a first minor one at about 2000 K (interval C) and a broad release over 2200 K (interval D) with a maximum at 2300 K, not related to that of Nd. The latter element is an indicator for the matrix vaporisation as it is an immobile and non-volatile fission product. In the MOX2 sample two very distinct Sr release peaks can be observed, the first one just below 2000 K and the second over 2200 K, the latter strongly correlated to that of Nd. This suggests that Sr is present in different phases, for example, the mixed oxide grey phase (Ba,Sr)(Zr,U)O_3 and as dissolved element in the UO_2 matrix.

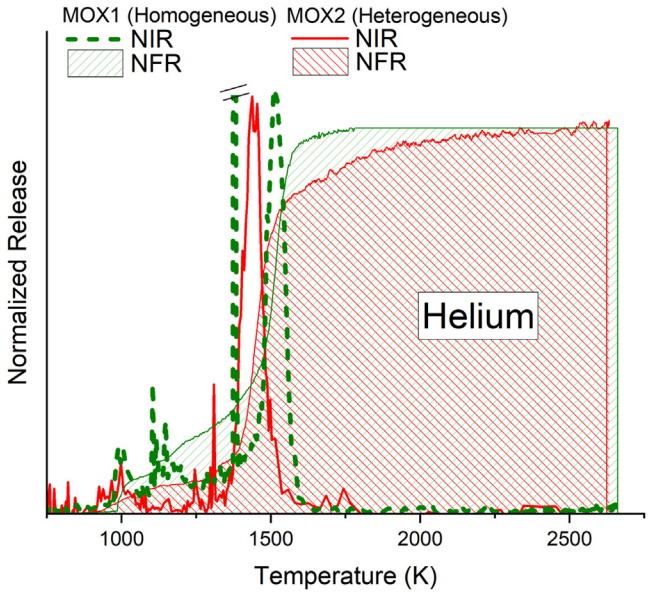

Fig. 11. Normalized Instantaneous and Fractional Release (linear scale) of Helium from MOX1 and MOX2.

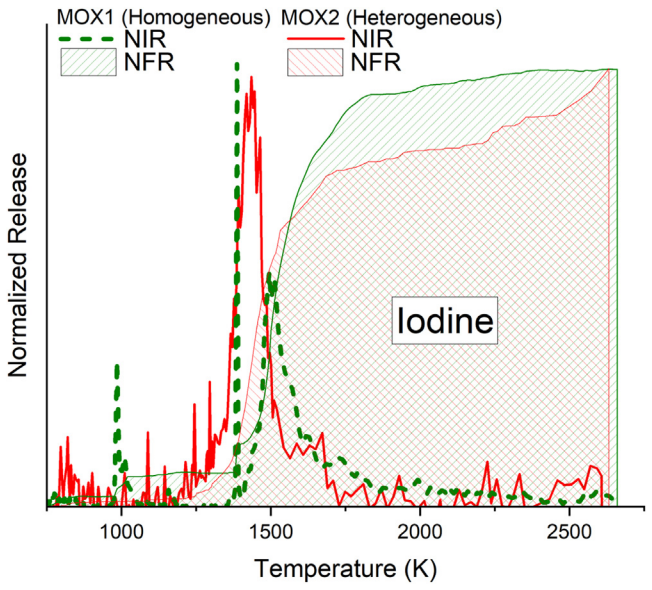

Fig. 12. Normalized Instantaneous and Fractional Release (linear scale) of Iodine from MOX1 and MOX2 (the NFR for the MOX2 over 1500 K has a high uncertainty due to low signal/noise ratio).

The similarities and differences are further evidenced in Figs. 9–15, in which the Normalized Instantaneous Release profiles are shown as the NIR; Eq. (3). The IR consist of the Intensity of the Release (IR) determined from Eq. (2). The IR corresponds to the differential effusion flow expressed in amount of vapour species per time at a given temperature normalised to the highest peak of the given release. The NFR, Normalised Fractional Release, Eq. (5), consists of the integral of the instantaneous release FR (Eq. (4)), at a given temperature normalised to the value at the end of the release. The Quantitative Relative Fractional Release (QRFR) correspond to the NFR multiplied by the quantity of the corresponding gas per gram of fuel released from the samples during the KEMS measurement and measured by the Q-Games.

$$IR = I\sqrt{T} \tag{2}$$

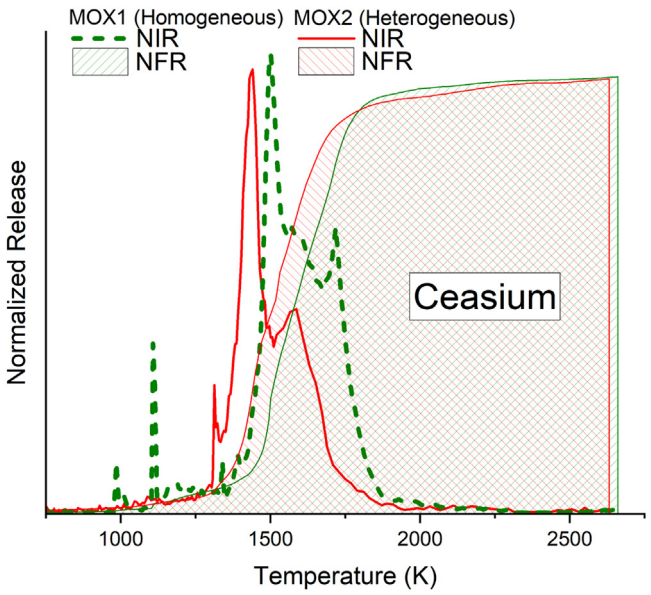

Fig. 13. Normalized Instantaneous and Fractional Release (linear scale) of Ceasium from MOX1 and MOX2.

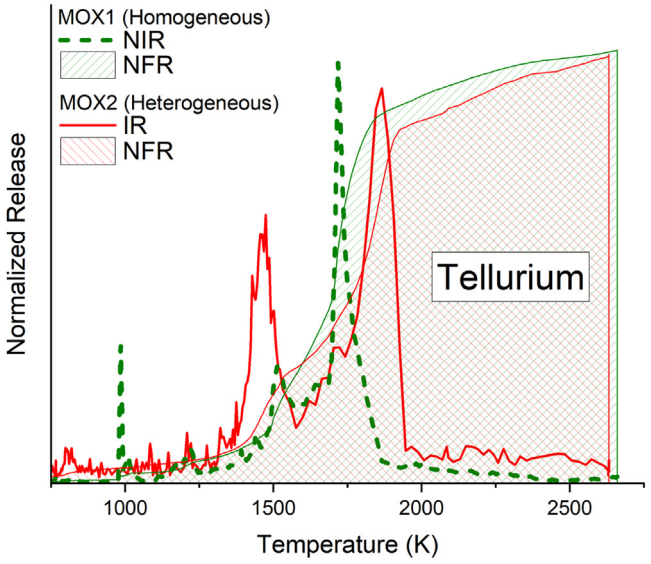

Fig. 14. Normalized Instantaneous and Fractional Release (linear scale) of Tellurium from MOX1 and MOX2.

$$NIR = \frac{I\sqrt{T}}{max\left(I\sqrt{T}|\forall T\right)} \tag{3}$$

$$FR = I\sqrt{T}dt \tag{4}$$

$$NFR(ti) = \frac{\int_0^{ti} I\sqrt{T}dt}{\int_0^{tend} I\sqrt{T}dt} \tag{5}$$

With I the mass spectrometer signal intensity in A, T the temperature in K, dt the time between consecutive measurements. Note that those equations are simplified for relative comparison.

For all fission products, the normalised release fraction in the homogeneous MOX1 fuel reaches a full release at much lower temperature than the heterogeneous MOX2. In most of the cases, with the exception for the Cs, it can be noted that the main release is very abrupt in the MOX1 sample whereas for the MOX2 it is more

Table 3
Quantitative measurement of the fission gases and Helium in the samples with the Q-Games.

	MOX1 (homogeneous) 2983 days after unload	MOX2 (heterogeneous) 1978 days after unload	Ratio MOX2 / MOX1
Xe quantity (mol/g_{fuel})	$1.21 \times 10^{-4} \pm 10\%$	7.09×10^{-5}	0.586
Kr quantity (mol/g_{fuel})	$7.71 \times 10^{-6} \pm 10\%$	3.47×10^{-6}	0.45
He quantity (mol/g_{fuel})	$8.95 \times 10^{-6} \pm 10\%$	7.88×10^{-6}	0.88

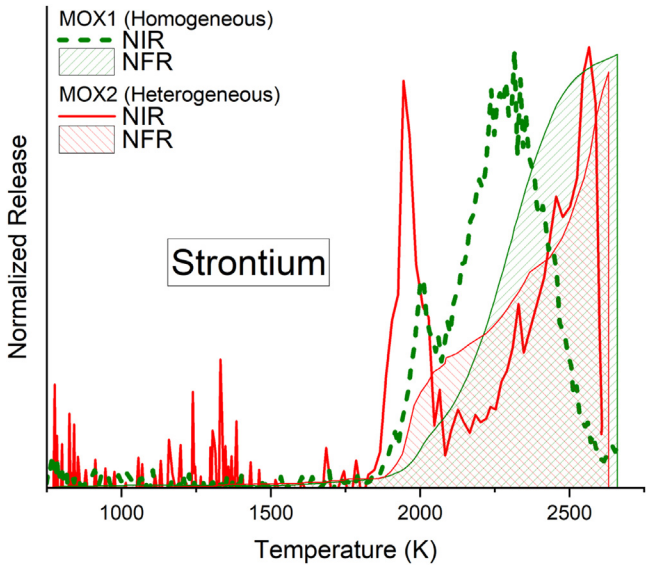

Fig. 15. Normalized Instantaneous and Fractional Release (linear scale) of Strontium from MOX1 and MOX2.

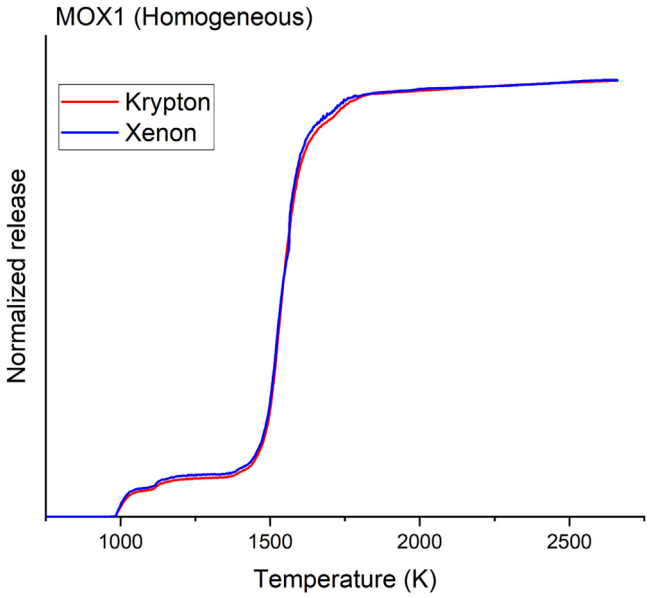

Fig. 16. Q-Games measurement data of Xenon and Krypton for the MOX1 (Homogeneous).

spread towards the higher temperatures. The onset of the main release remains however at the same temperature.

For Xe, Kr, and I the full release in the homogeneous fuel occurs approximately immediately after the major release, in the heterogeneous fuel there is still a significant release between the major release and the full vaporisation of the sample. In contrast, the normalised release fractions of Cs and Te are very similar for the two fuels. As shown by Figs. 9–15, the main peak of the red coloured release curves (heterogeneous MOX2) are consistently shifted to lower temperature, except for the noted high-temperature release of Sr.

3.2. Quantitative measurement of fission gases and helium

The fission gas and helium retained in the samples have been quantitatively measured during the laboratory anneals. The experiments for MOX1 and MOX2 were performed 2983 and 1978 days after fuel unload, respectively. After the complete vaporisation of the matrix, the total quantity of Xe, Kr and He released was determined with the Q-Games.

Table 3 shows the quantities measured. The quantity of helium generated after irradiation until the measurements has been assessed from the actinides inventory and the decay engine from NUCLEONICA™ [28]. About 2×10^{-5} and 1.5×10^{-5} mol.g^{-1} of helium were formed during storage of MOX1 and MOX2 respectively. Due to technical difficulties during the measurement of the MOX1, the standard precision of ± 1% for the Q-Games instrument [21] cannot be guaranteed. We estimate a precision of ± 10% for those values. This could explain the difference of ratio between the quantity of Xe and Kr in each MOX in Table 3.

The results show clearly that the MOX2 (Heterogeneous) contains only about half of the fission gas compared to MOX1. This is due to the larger FGR% during irradiation of MOX2 (Table 1). The helium concentrations are closer, but this is because a large fraction of this helium originates from the alpha-decays of the actinides after the end of reactor irradiation. The total quantities of helium measured for MOX1 and MOX2 are comparable with the calculated values of helium generated by decay during storage (about 8 and 6 years respectively) which indicates that the fraction produced during irradiation was not present anymore. The quantity of the helium in both fuels does not exactly match with the expected quantity and one could speculate that the microstructure was responsible for a partial release during storage, i.e. higher for the fully restructured sample (MOX1).

3.3. Microscopic examinations

3.3.1. MOX1 after annealing experiments

SEM of the irradiated MOX 1 sample showed the clear formation of HBS. The original grain size of about 10 µm in the fresh fuel (Fig. 1) changed to less than 1 µm after irradiation (Fig. 19b), with the characteristic porosity surrounded by sub-µm polygonal grains. Such a structure is in line with the high burnup (≥ 100 MWd/kgHM) associated to a low irradiation temperature (973 K), which prevents grain growth [29]. EPMA showed a homogeneous distribution of the fission products and Pu (Fig. 25), with some Xe retained in bubbles and spots of high Mo concentration probably along a pellet crack. This Mo is likely coming from local interaction with the Mo disks separating the pellets. For the heterogeneous MOX2 sample, EPMA has been performed to assess quantitatively the distribution of U, Pu, Nd, Xe, Cs, Mo, and Ru in the irradiated fuel before annealing and measurement by KEMS. The images (Fig. 26) show that it had retained its fresh fuel microstructure (Pu rich islands in the UO_2 matrix). As stated above, additional MOX1 fragments were annealed in the KEMS up to 1250 K, 1520 K and 2000 K. After each temperature step, samples were examined

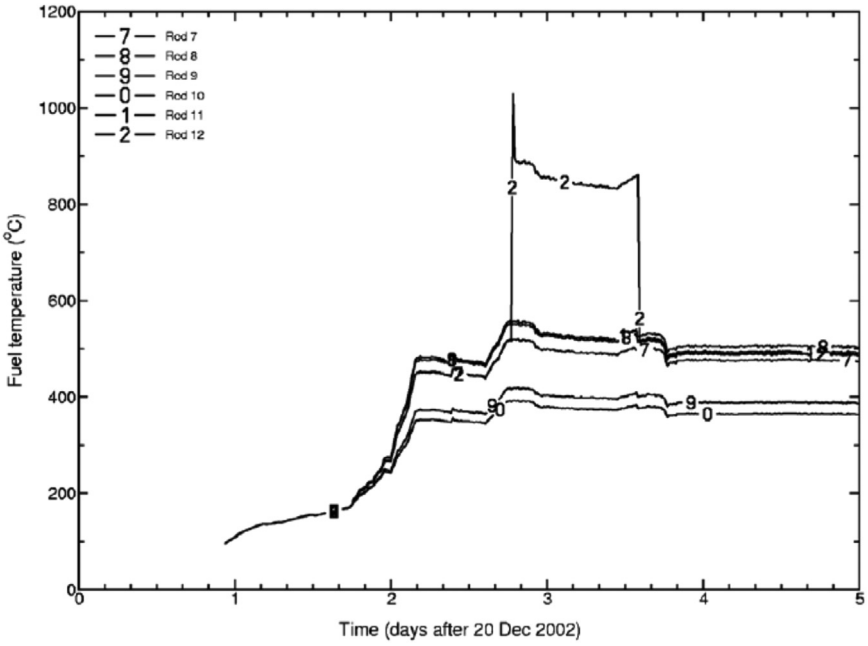

Fig. 17. Temperature increase in rodlet 12 following the December 2002 reactor restart (from[13]).

by SEM. No fragmentation of the samples were observed. However, given the small size of the sample it does not demonstrate that no fragmentation would occur with bigger samples. Fig. 19a-h shows a sequence of SEM images recorded at the various steps of the annealing process. Two magnifications have been selected to evidence the microstructural changes. Fig. 19 shows the typical HBS structure i.e. small grain of about 250 nm and a typical micrometric porosity is mostly preserved up to 1520 K.

After heating at 1250 K the structure remains basically the same with micro and submicrometric grains shown in the SEM micrographs Figs. 19c,d and 20. In addition some smaller than typical (~150 nm) rounded sub-grains can be observed in the micrometric pores. The inset in Fig. 20 shows a STEM image of the sample revealing rounded grains of less than 50 nm (as shown by the arrow). A clear modification of the grain edges is visible, sharp edges became rounded. At this temperature already 8% of the gas has been released in the KEMS measurement (Fig. 9). This gas was probably released from the grain boundaries, from the volume near the surface of the grains and cracks of the studied small fragment. This has been also described by White in particular referring to the S/V ratio considering the fractal nature of the open surface in UO_2 [16] and the fractal dimension on the surface of rounded grains in the HBS [16,29]. In some TEM images nanometric bubbles (already present after irradiation as previously observed in high burnup fuels [29]) could be identified together with epsilon particles (metallic precipitates containing Ru, Rh, Mo, Pd, Tc) as shown in Fig. 21a,d but also in Fig. 22 in more details. Fig. 21g shows the presence of dislocation lines in some cases tangled. This confirms the very beginning of the diffusion and precipitation of fission gas in the matrix.

After annealing at 1520 K, the structure starts to change, the grains show some more pronounced rounding of the edges with sometimes visible gaps between them due to thermal etching (Fig. 15f). The very small rounded nanometric grains have disappeared, which is attributed to surface diffusion. However most of the microstructural features have not changed and the porosity, for example, is still of the same order as in the original sample. At this temperature, the fission gases can diffuse inside the grains to reach the boundaries or be trapped in intragranular bubbles. Fig. 17b,e shows that the intragranular bubbles have grown and dislocation lines are still visible (Fig. 17h). About 50% of the fission gas inventory has been released, rapidly increasing to 80% at 1600 K and 95% at 1800 K.

At 2000 K the structure has completely changed (Fig. 19g,h). The pores have increased in size while reduced in concentration, and the grains have grown, as expected. Some intragranular bubbles can be observed by STEM in some of the grains (Fig. 21c). Fig. 19f shows in particular the presence of rounded precipitates similar to the observation by SEM. The intragranular bubbles probably contain the 5% of gas released between 1800 K and the complete vaporisation of the sample. Note the appearance of light particles at the surface of the sample (Fig. 19h), which have been identified by EDX measurements as epsilon particles mixed with W coming from the liner of the Knudsen cell. Fig. 21j-l shows the composition measured by EDX of some of these particles. At the higher temperature of 2000 K the Tc content has dropped.

3.3.2. Microscopic examinations of MOX2 after irradiation

A complete study of the microstructural behaviour with temperature of a MOX fuel sample with a comparable microstructure and release behaviour to MOX2 has been published earlier [30]. In the sample reported in that reference, the Pu agglomerates at the radial periphery had a burnup of about 270 MWd/kgHM and the matrix a burnup of about 13 MWd/kgHM. Its irradiation temperature was slightly higher than the MOX2 sample reported in this paper (around 1100 K). The most important observations from that study can be summarised as follows:

- The microstructural evolution of the Pu-rich areas is very similar to that of the HBS described for MOX1, with little change up to 1300 K, after which the rounding of grains edges and grain boundary opening start. At 1600 K restructuring starts, which is accompanied by grain growth and pore aggregation. At 2100 K an open structure is formed.
- The microstructural evolution of the matrix shows grain boundary opening around 1450 K and the formation of elongated and connected pores at the grain boundaries at 1800 K.

In the work presented in this paper, EPMA measurements of the irradiated MOX2 sample were made on a polished sample in order

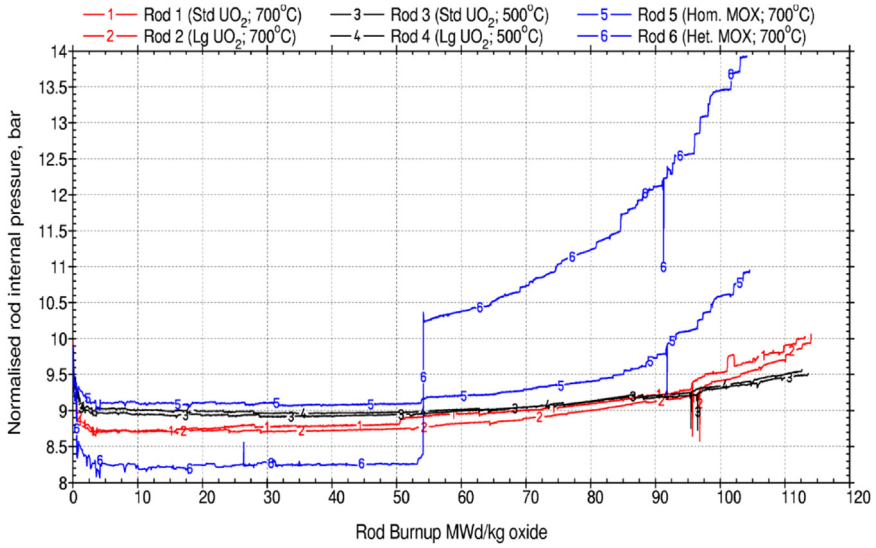

Fig. 18. Normalised in-pile pressure data from the sibling MOX rodlets in the lower cluster (rod 5 equivalent to rod 10 and rod 6 equivalent to rod 12 in the upper level respectively) (from [13]).

to get quantitative information on the distribution of Xe, Cs, Mo, Nd, Ru, Pu and U. The results are shown in Fig. 26. Those measurements revealed the following information:

- From the Nd concentration the peak local burnup of a Pu-rich area vs the U-rich area could be estimated as 341 MWd/kgHM and 25 MWd/kgHM.
- The Xe concentration map shows the presence of very little quantities of Xe in the Pu-rich areas implying that the Xe originating from those areas was released during irradiation (HBS formation). At the edges and outside of the Pu rich regions, where the threshold burnup for HBS formation was not reached, the Xe was retained in the matrix. Some bubbles filled with Xe can also be seen on the map. It shows a higher concentration of Xe in the U-rich area, which probably has been produced by the fission of the Pu bred from the ^{238}U during the irradiation. The areas with the higher Xe concentration adjacent to Pu-rich areas within a few µm correspond well with the expected range of recoil for such a heavy fission product in UO_2 (about 7 µm). This suggests that some Xe originating from the Pu-rich areas has been implanted in the UO_2 matrix and did not diffuse further during irradiation.
- The Cs concentration map shows that in contrast to Xe this element is still present in the Pu-rich areas.
- The distribution map of Mo correlates with Nd and Cs and shows a concentration in the Pu-rich areas, where also some particularly high concentration spots correlate with Ru. This suggests that a significant fraction of Mo is in the matrix but some is in the five-metal epsilon particles, in line with the suggested Mo/MoO_2 oxygen potential buffering of this element.
- The concentration map of Ru reveals that it is concentrated in spots, likely corresponding to epsilon particles. It is worth noticing that the Ru-rich spots do not always corresponds to a high concentration of Mo, suggesting on that the composition of the particles varies within the fuel.

3.4. Thermal diffusivity measurement

Thermal diffusivity measurements of MOX1 were carried out during three annealing cycles with maximum temperatures of 660 K, 740 K and 830 K (Fig. 23). A thermal diffusivity recovery was observed after each run. The sample started to fragment during the fourth measurement run while temperature was being increased up to about 930 K. This temperature is close to the irradiation temperature of the fuel.

For MOX2, four annealing cycles were performed with maximum temperatures of 670, 750, 840 and 1020 K (Fig. 23), showing a similar thermal diffusivity recovery after each run. The sample started to fragment during the fifth measurement run while temperature was being increased up to about 1050 K.

Fig. 24 shows the thermal conductivity of the homogeneous and heterogeneous MOX as a function of temperature, normalised to 5 vol.% porosity using Eq. (1). The porosity volume fraction was deduced from the ratio of the irradiated fuel real density (measured by the Archimedes method) to the irradiated fuel matrix density. The irradiated fuel matrix density was calculated from the fresh fuel theoretical density corrected according to [31] for the matrix swelling due to solid fission products (0.32% per 10 GWd/tHM) and due to retained fission gases (0.56% per 10 GWd/tHM, to be multiplied by the fraction of retained fission gases). The fraction of retained fission gases was deduced from the values of FGR from puncture data provided in Table 1. The irradiated fuels densities were 9.18 g.cm^{-3} for MOX1 and 9.39 g.cm^{-3} for MOX2 which led to porosity volume fractions of 9.8% for the homogeneous MOX1 fuel and 9.7% for the heterogeneous MOX2 fuel. The thermal diffusivity results after annealing (the highest values for each temperature) are close, and the homogeneous fuel showing a slightly higher thermal diffisivity. Fig. 24 shows a comparison of the thermal conductivity of MOX1 and MOX2 samples to irradiated UO_2 at 104.5 GWd/tHM obtained by a series of laser-flash measurements by Ronchi et al. [32] (with an irradiation temperature of 970 K) and the thermal conductivity of irradiated UO_2 as derived from in-pile centreline temperature measurements in the Halden Reactor Project [33]. The thermal conductivity of the current MOX samples is significantly higher.

4. Discussion

4.1. Fission gases and helium

The first observation to discuss is the behaviour of the fission gasses that were present in the fuel after irradiation. The gas release (Xe, Kr) during irradiation of the two rods 11 and 12 was not monitored, but the release fractions for sibling rodlets in the lower cluster of the irradiation capsule (see Section 2.2) was 25% for

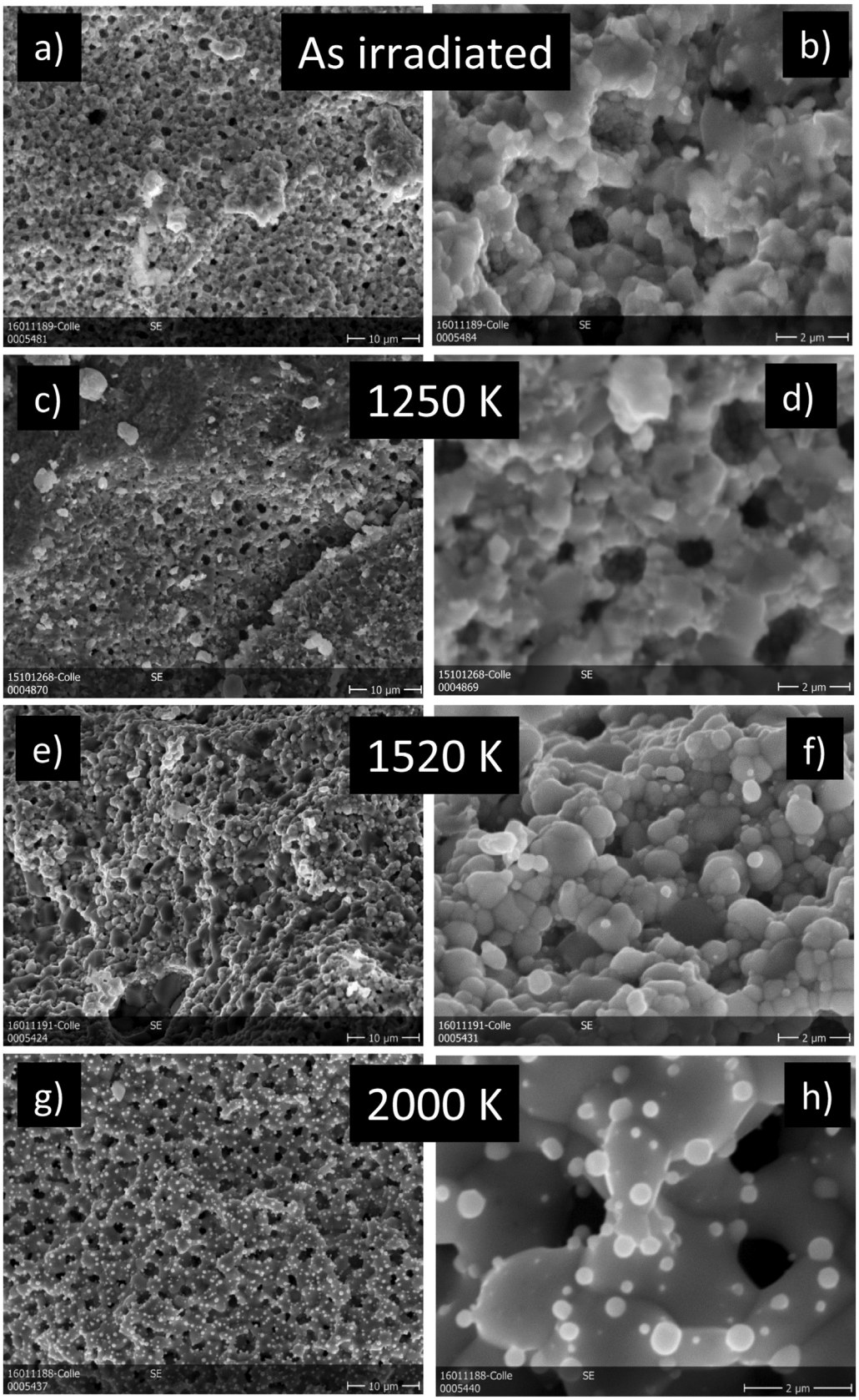

Fig. 19. Sequence of SEM pictures at two magnifications from MOX1 a,b) as received (as irradiated) and after annealing c,d) at 1250 K, e,f) 1520 K and g, h) 2000 K.

MOX1 and 60% for MOX2, see Table 1. As shown in Figs. 9 and 10, in the KEMS measurements, the main release of Xe and Kr takes place at lower temperature in the heterogeneous MOX2 fuel than in the homogeneous MOX1. In contrast, the homogeneous MOX1 fuel, which had a high-burnup structure, showed low-temperature spikes that were not observed in the heterogeneous fuel. These spikes could be related to burst release from gas bubbles near the surface of the full HBS structure of the MOX1 sample, and/or from (micro-) cracks forming upon heating. On the other hand, the fact that the MOX2 fuel operated for 24 h between 800 and 900 °C and went up to 1000 °C for a very short period at a burnup of ~40 MWd/kgHM, as mentioned in Section 2.2 [7], the same effect in that fuel could have been partly removed during irradiated, as a pressure jump can be seen during the online fission gas release monitoring.

The MOX2 still shows a substantial release between the major release peak and the complete vaporisation of the sample. In MOX2 the HBS developed only in the Pu rich areas, and the matrix kept its original microstructure. Moreover, at the low irradiation temperature in reactor (973 K) the diffusion of the gases was probably limited. Thus, fission gas generated in the matrix of MOX2 was still present after irradiation, as clearly seen from the EPMA mapping of Xe in Fig. 26. It should be noted here that typically EPMA cannot detect Xe in larger gas bubbles, and the low concentration of Xe in Pu-rich areas should thus not be interpreted as complete absence of this element [34]. As observed in Fig. 19 the MOX1 sample developed the HBS structure throughout the whole disk, and thus had a high density of grain boundaries as well as gas intergranular bubbles therefore with little gas remaining in the grains.

Table 3 shows that the heterogeneous MOX2 has a lower residual gas content (about half) compared to the homogeneous MOX1. This is consistent with the results of the fission gas release measurements during the reactor irradiation [7], during which rodlet 12 experienced high temperature at a burnup around 40 MWd/kgHM for approximately 24 h due to mal-operation of the gas flow system [7] as shown in Fig. 17. During this incident, the estimated peak temperature in rodlet 12 (with MOX2) could have reached values above 1000 °C and the subsequent short-lived fission gas release measurements showed clear indications of interlinkage on this rodlet. The evaluated release-to-birth and surface-to-volume ratios remained high for this rodlet for the remainder of the irradiation after this temperature excursion event.

It is interesting to also compare the in-pile pressure data from the sibling MOX rodlets from the lower cluster, since they, as stated above, had a very similar power history to the two rodlets from which the disc examinations documented here were performed. The normalised pressure curves for these rodlets showed no significant fission gas release below a burnup of ~62 MWd/kgHM, at which point the pressure in rodlet 6 (with MOX2 fuel) showed an abrupt jump as can be seen in Fig. 18. The pressure increase became evident above ~96–101 MWd/kgHM. From these pressure data in the lower rodlets cluster, the in-reactor fission gas release values were derived as 17% for rodlet 5 with homogenous MOX1 and 47% for rodlet 6 containing heterogeneous MOX2 (Table 1), which suggest a residual gas ratio of 0.64, slightly higher than the value observed for Xe, the major fission gas. This is of course an overall value for the pins with sibling fuel and near identical power histories, whereas the values reported in our work refer to a local sampling.

Helium is different from the fission products because it is also generated in the fuel during cooling due to alpha decay and has a much larger diffusion coefficient. The cooling time prior analyses of the MOX2 sample was shorter than MOX1 sample (65 vs 98 months, i.e. a ratio of 0.663). The release curves of helium (see Fig. 11) are very similar to those of the fission gases, showing

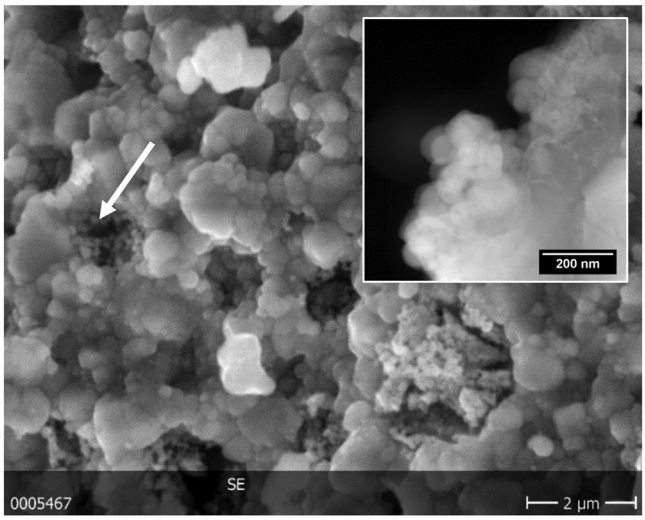

Fig. 20. SEM micrograph of the MOX1 sample after annealing at 1250 K. The inset show a STEM image showing the very small rounded grains as shown for example by the arrow in the SEM micrograph.

also the 100 K earlier release between MOX2 and MOX1. It should be noted that in the case of the heterogeneous MOX2 there is a fraction of helium that is released around 1100 K and which is not present in the release curve of the homogeneous MOX1. The release of this fraction could be attributed to the helium produced during cooling and located likely in the matrix compared to the gas that has migrated and precipitated concomitantly with the fission gases in the homogeneous fuel during irradiation [35]. This is consistent with measurements of irradiated fuel showing that helium is partially retained in fuel with HBS up to about 1750 K [30].

It can thus be concluded that the fission gas release from the heterogeneous fuel is larger and starts at lower temperature compared to homogeneous fuel with full HBS structure. In the heterogeneous fuel the gas is mainly generated in the Pu-rich areas with HBS structure that have very large local burnup. Due to the highly porous HBS structure and the fracturing of matrix, the gas can be released easily and is not limited by grain boundary diffusion through the matrix. However, the Xe generated in the matrix of the heterogeneous fuel is only released at higher temperature, typical for its low local burnup [36], and is likely related to small intragranular bubbles, as observed by TEM in this type of MOX fuel [30].

The behaviour of krypton and xenon is usually quite similar. However, for the MOX1, the NIR of Krypton as shown in Fig. 9 does not perfectly match the one of Xenon in Fig. 10. For example the spikes at about 1050 K appear on the Xenon release but not on the Krypton one. This is due to the fact that each mass is measured for half a second every 2–3 min, so that the Xenon spike was already terminated when the measurement for Krypton started. However, the Q-Games data in Fig. 16 clearly show both spikes and a similar behaviour for both gases could be concluded.

4.2. Other fission products

The other fission products are concentrated in the Pu-rich areas in the heterogeneous MOX2 fuel as can be seen from the EPMA maps of Cs and Mo in Fig. 26. They are more homogeneously distributed in the MOX1 as shown in Fig. 25. The normalised release curves of Cs of MOX1 and MOX2 are very similar, with a shift between the two fuels, similar to the fission gases. The Cs release occurs in multiple maxima in the mid-temperature B interval (1300–1650 K) in which intergranular and intragranular diffusion dom-

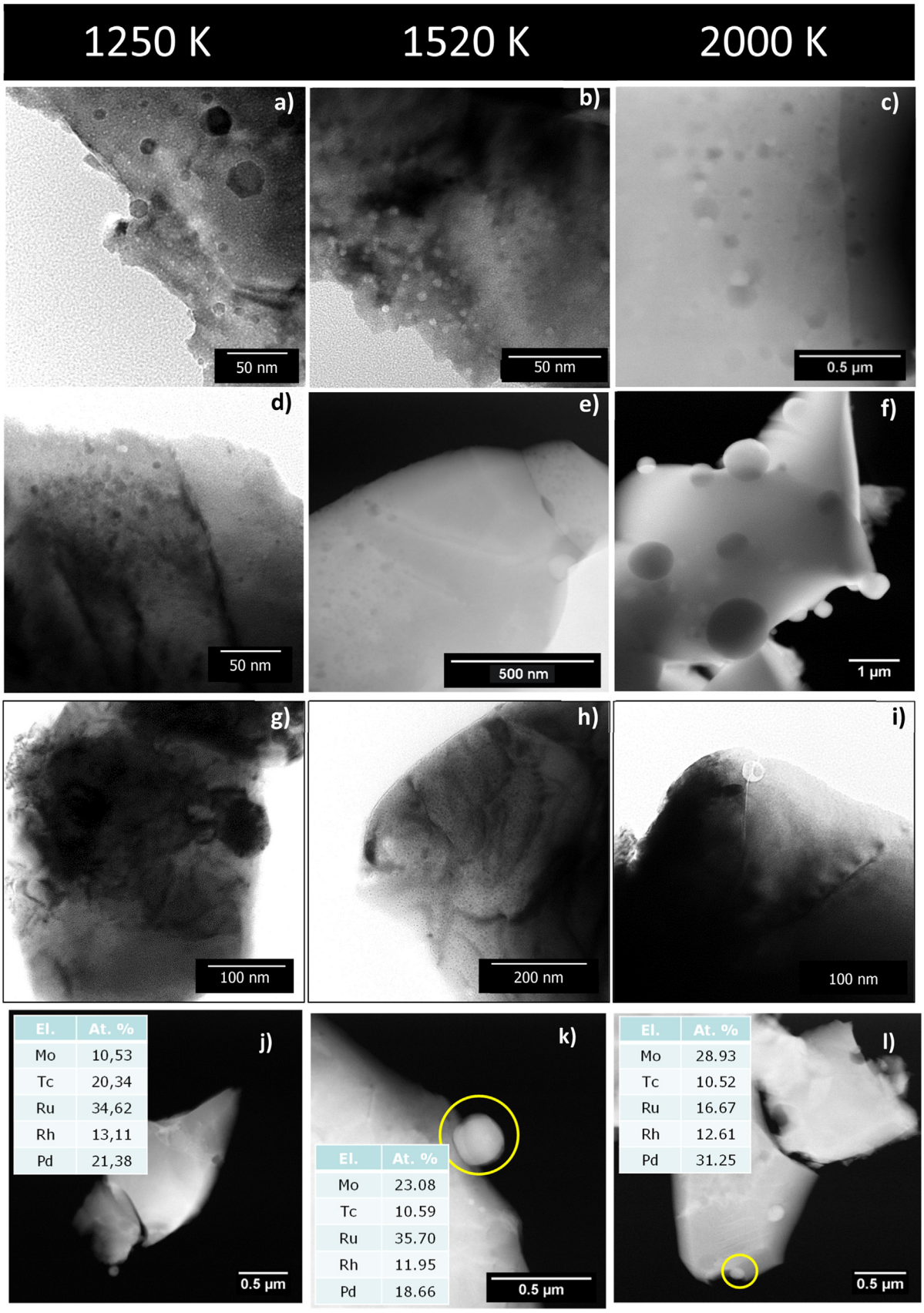

Fig. 21. TEM bright field images of the MOX1 annealed samples at (a, d, g, j) 1250, (b, e, h, k) 1520 and (c, f, I, l) 2000 K respectively.

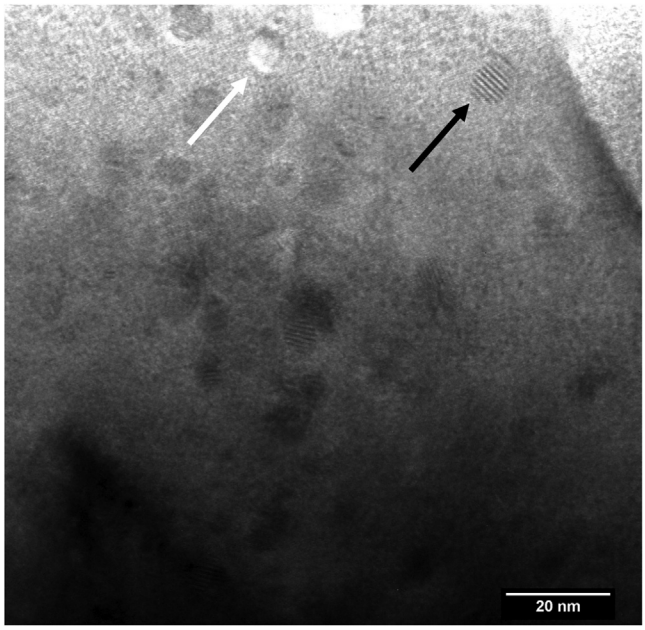

Fig. 22. TEM micrograph of MOX1 sample after annealing at 1250 K Showing the presence of nanometric bubbles (small bright spots shown for example by a white arrow) as well as epsilon particles (larger darker polyhedral spots with Moiré fringes, shown for example by a black arrow).

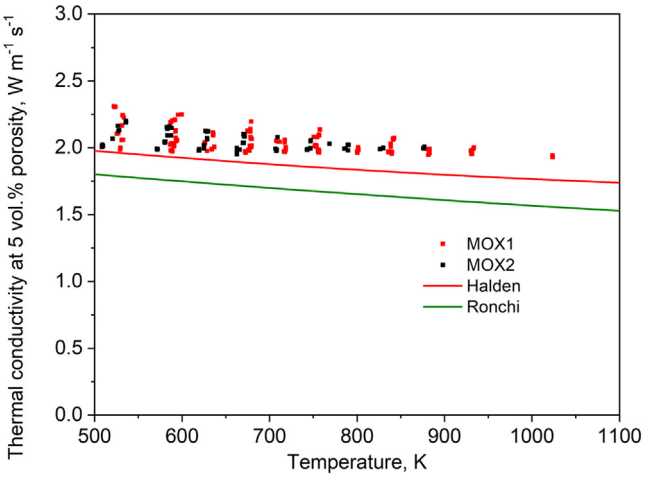

Fig. 24. Thermal conductivity (normalised to 5 vol.% porosity) of the homogeneous and heterogeneous MOX as a function of temperature and comparison to the predictions of the formulas for UO_2 at 104.5 GWd/tHM of Ronchi [32] (with an irradiation temperature of 970 K) and of the Halden Reactor Project [33].

inate and grain boundaries start to open, as demonstrated in systematic heating studies of MOX fuel [30]. Since the main maximum release of Cs at about 1500 K in coincides with the release of Xe, Kr, and I in both fuels, it is likely related to its transport along the grain boundaries from the HBS zones. It is shifted by about 70 K between MOX1 and MOX2. The second clear maximum that follows and partially overlaps with the first one and a weak release in between, is shifted more substantially, about 150 K and represents the intragranular diffusion of Cs to the grain boundaries in the HBS zones. Since in the homogeneous MOX1 this strong maximum of Cs at 1720 K coincides with a strong Te signal, it suggests that the mobility of Cs is related to different mechanisms/species. This is not surprising as the Cs fission yield is much higher than that of other elements such as I or Te, and therefore it can be associated/bonded with multiple elements. The heterogeneous fuel shows minimal Cs release above 1700 K, in contrast to the fission gases, indicating that only a limited fraction of the Cs produced remained dissolved in the matrix or in nanobubbles.

The release curves of Iodine from the two fuels are very similar to those of the fission gases with a similar temperature shift, indicating a similar behaviour. It can be noted that the spike release of Iodine in the interval A of MOX1, corresponds to the Xe signal. It only slightly correlates to the very weak Cs signal whereas Iodine spikes are absent for strong Cs spikes. This suggests there is no association of the two elements (e.g. CsI). Also the strong low-temperature spike in the release curves of Te in MOX1 correspond to Xe but not Cs. Te is, however, different from Xe, I and Cs because the shift of the curves between MOX1 and MOX2 is not systematic as in the other cases. The release peak at the highest temperature occurs significantly higher in the heterogeneous MOX2 and is not associated with Cs release as in MOX1, suggesting a different chemical origin. This could suggest that Te is present in various forms in MOX2, labile and bonded. For example, in the high-burnup Pu-rich areas of MOX2, Te might be partially bonded in the five metal particles, as observed for example in UO_2 fuel [37], whereas it might be still elemental in the matrix where it is much more diluted or associated with Cs, for example as a caesium telluride.

The release of Sr occurs in the very high temperature range (2000–2500 K) and shows two maxima, but again different for MOX1 and MOX2. In the homogeneous fuel, the two maxima are close in temperature and the release is terminated before the complete vaporisation of the sample. In the heterogeneous sample, the

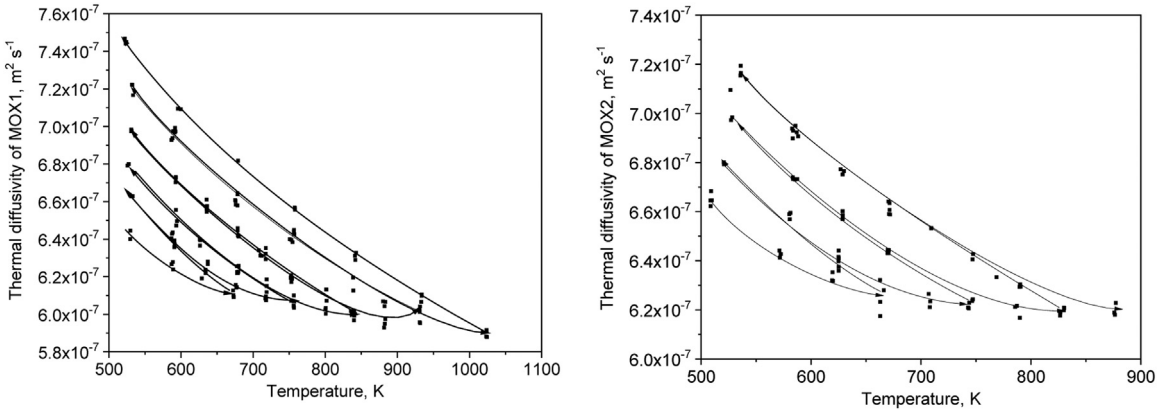

Fig. 23. Thermal diffusivity measurement cycles with increasing maximum temperature of the homogeneous MOX1 (left, rod 11) and heterogeneous MOX2 (right, rod 12).

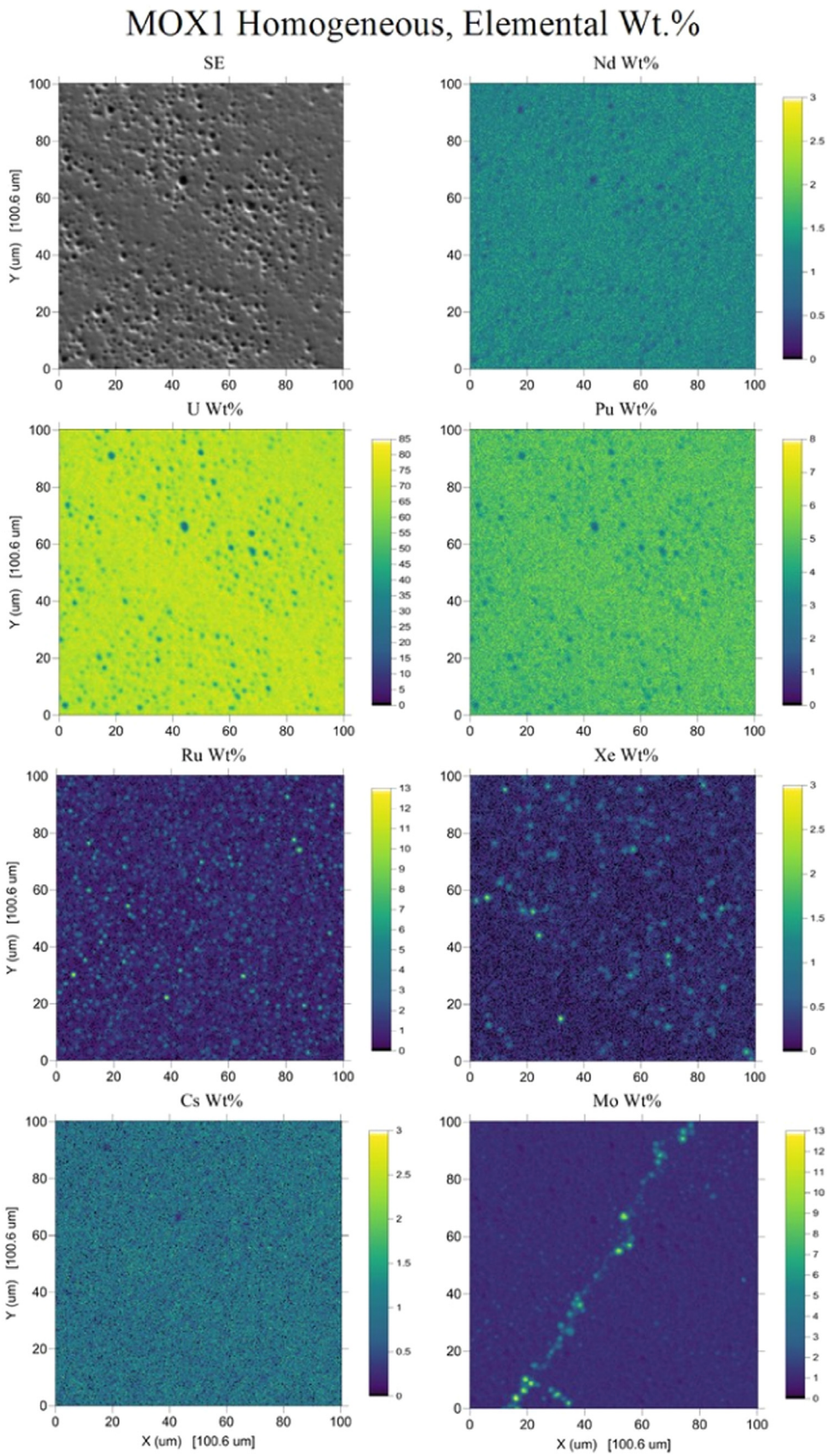

Fig. 25. EPMA of the homogeneous MOX1 fuel after irradiation. Top left image: SE = Secondary Electron image.

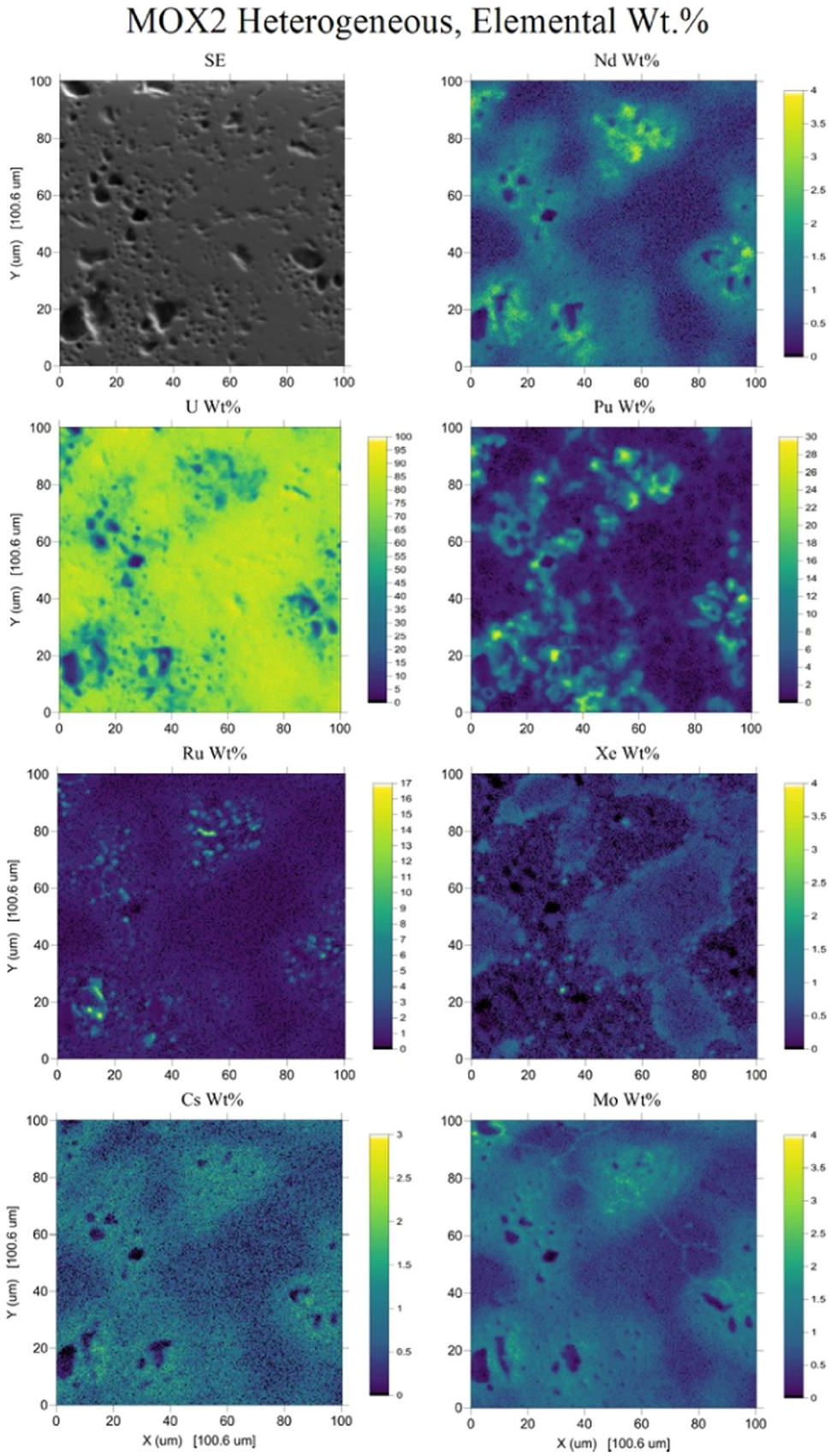

Fig. 26. EPMA of the heterogeneous MOX2 fuel after irradiation. Top left image: SE = Secondary electron image.

two maxima are clearly separated by more than 500 K, indicating again distinct different mechanisms or species.

4.3. Comparison with commercial PWR fuels

In previous studies we have measured the fission product release from fragments of commercial UO_2 fuel with HBS structure ([37], results from this reference are shown in Fig. 8 in this paper), and of fragments of OCOM MOX fuel from different radial locations in the pellet ([30], results shown in Fig. 7).

The microstructure of MOX1 studied here is very similar to the one of the HBS UO_2 sample with a local burn-up of about 240 MWd/kgHM. The release behaviour from the two fuels is comparable, including the above noted correlations between the fission products. However, the Cs release in the UO_2 fuel continued to higher temperatures which could be explained by a higher oxygen potential at which caesium is no longer present in a volatile form (Cs, CsI) but bonded in oxide form, for example caesium molybdate, caesium uranate or a more complex oxide compound [37].

The fission gas release curves of commercial OCOM MOX fuel reported in [30] (sample A, irradiation temperature between 854 and 1312 K, fuel burnup 44.5 MWd/kgHM, local burnup $>$ 200 MWd/kgHM) shows a somewhat different behaviour from MOX2. The Xe curves show a first release at about 1200 K, lower than observed here for MOX2, and at high temperature ($>$ 1500 K) the release is substantially larger. This can be explained by the difference in the Pu distribution in the fuel. In the commercial MOX fuel the Pu concentration is higher in the matrix and lower in the Pu-rich areas compared to the heterogeneous sample studied here. The local burnup of the matrix is thus higher resulting in (i) a larger fission gas concentration at the grain boundaries, and thus a faster (lower temperature) grain boundary opening, and (ii) larger concentration of fission gas still contained in the matrix (dissolved, nano- and microbubbles) which is only released at high temperature.

The particular behaviour of Te and Sr, both showing a shift in release to higher temperature in the heterogeneous MOX2 fuel in comparison to the commercial MOX fuel, can be explained by the fact that in this fuel the Pu areas change substantially their composition during the irradiation. An average fuel burnup of about 44.5 MWd/kgHM means that about one-third of the Pu and U in as a result of the much higher Pu concentration. Pu-rich areas is replaced by fission products, resulting in about 50 at% concentration of new elements. At such high concentrations, in combination with short diffusion paths and elevated temperatures, reactions can take place rapidly, and we hypothesize that new phases are more likely to form, as observed in fast reactor fuel [38], which volatilize at relatively low temperature. The high release temperature of Te may be related to its incorporated in the five-metal particles in which it may be strongly bonded to Pd [39]. Finally, Sr in the Pu areas will be incorporated in a grey-phase-like perovskite type $(Ba,Sr,\ldots)(Pu,Zr,\ldots)O_3$ from which the Sr is released at higher temperature than when dissolved in the fluorite matrix. Generally the formation of compounds between Pu and FPs is still matter of investigation and local oxygen potential and low FPs and Pu ratio might impact the local chemistry.

4.4. Correlating fission gas release and thermal diffusivity measurements

An interesting aspect is the correlation between the fission gas release and the observations made during the thermal diffusivity measurements. As discussed in Section 3.4, the thermal cycling of the samples during the laser-flash measurements results in an annealing of radiation damage accumulated in the fuels. This was discussed extensively by Ronchi et al. [32], who indicated that distinction should be made between the annealing of defects resulting from self-irradiation during the storage (out-of-pile) of fuel between end-of-life and measurement, and the annealing of defects created during the irradiation period (in-pile) of the fuel. The irradiation temperature T_{irr} is a key parameter in this interpretation. Below T_{irr} the out-of-pile self-irradiation defects dominate, as annealing of in-pile defects has taken place, above both have to be taken into account.

The fuel disks studied here were irradiated at a constant temperature of $T_{irr} = 973$ K. The homogeneous MOX1 fuel fractured at about 930 K, close to the temperature at end of irradiation, also corresponding to the temperature range in which the first burst release of fission gases was observed in the KEMS. Thus, we hypothesize that the annealing of the defects mobilised the helium from the out-of-pile decay and remaining fission gases in the HBS matrix, their mobility led to sudden release by venting of overpressurised intergranular HBS bubbles and (saturated) grain boundaries and, hence, to destabilisation of the fuel disk. The MOX2 fracturing took place at about 1050 K, above T_{irr} and the KEMS showed no burst release in that temperature range. Since the fission gas release in MOX2 starts only at higher temperature, the mechanical destabilisation of the fuel disk must be due to a different mechanism, probably involving the growth of intergranular pores in the matrix and local swelling of the Pu-rich areas.

5. Conclusion

The distribution of plutonium in mixed oxide fuel has a strong influence on the fission product release when the fuel is heated, as has been demonstrated in this study by examining two extreme cases: a fully homogeneous and a highly heterogeneous MOX fuel. KEMS measurements of irradiated fuel samples combined with SEM imaging of the fuel during various stages of the heating and EPMA analysis show that the differences in the Pu concentration and the concomitant differences in burnup distribution affect the microstructure evolution (local or uniform HBS formation) as well as the fission product concentration in Pu-rich areas, matrix and grain boundaries, and thus the release mechanisms. The main release of fission products from the homogeneous and heterogeneous fuels takes place at about the same temperature. i.e. around 1500 K. The slightly lower temperature in the heterogeneous fuel can be related to the extreme burnup and restructuring of the Pu-rich areas, and higher mobility along the grain boundaries of the surrounding matrix resulting from the substantially higher in-pile gas release. In the homogeneous fuel, spike release of fission gases and volatiles takes place at a lower temperature, probably because of the full HBS development and release from near surface pores. The most prominent differences are observed for Sr, Te and Cs, which were attributed to differences in chemistry in the Pu-rich areas that have an extremely high burnup and FP concentration, very likely resulting in a more extensive chemical interaction.

Declaration of Competing Interest

The authors declare that they have no known competing financial interests or personal relationships that could have appeared to influence the work reported in this paper.

CRediT authorship contribution statement

Jean-Yves Colle: Writing – original draft, Investigation. **Thierry Wiss:** Writing – original draft, Investigation. **Oliver Dieste:** Investigation. **Philipp Pöml:** Writing – original draft, Investigation. **Dragos Staicu:** Writing – original draft, Investigation. **Terje Tverberg:** Writing – original draft. **Stéphane Bremier:** Writing – review & editing, Resources. **Rudy J.M. Konings:** Writing – original draft.

Vincenzo V. Rondinella: Writing – review & editing, Resources. **Takeshi Sonoda:** Writing – review & editing. **Akihiro Sasahara:** Writing – review & editing. **Shoichi Kitajima:** Writing – review & editing.

Data Availability

Data will be made available on request.

Acknowledgments

The authors would like to acknowledge Jérôme Himbert and Bert Cremer for their support to the micro-analysis of the samples, Anette Küst and Eckhart Dahms for the support to the thermal diffusivity measurements, and Gérard Montagnier for the preparation of the samples.

The fresh fuel samples, which were irradiated for this study, and the results of their characterisation were provided by the NFIR program (https://www.epri.com/portfolio/programs/108031). The authors thank the NFIR members for permission to publish the results.

References

[1] D. Staicu, R.J.M. Konings, T. Wiss, O. Beneš, C. Guéneau, J. Noirot, Plutonium in nuclear fuels, Pluton. Handb. (2019) 2312–2321.
[2] G. Oudinet, I. Munoz-Viallard, L. Aufore, M.-J. Gotta, J.M. Becker, G. Chiarelli, R. Castelli, Characterization of plutonium distribution in MIMAS MOX by image analysis, J. Nucl. Mater. 375 (1) (2008) 86–94.
[3] Status and Advances in MOX Fuel Technology, International Atomic Energy Agency, Vienna, 2003.
[4] C.T. Walker, W. Goll, T. Matsumura, Further observations on OCOM MOX fuel: microstructure in the vicinity of the pellet rim and fuel — Cladding interaction, J. Nucl. Mater. 245 (2) (1997) 169–178.
[5] H. Bairiot, J.V. Vliet, G. Chiarelli, J. Edwards, S.H. Nagai, F. Reshetnikov, Overview of MOX fuel fabrication achievements, Int. Atom. Energy Agency (2000) Vienna (Austria); OECD Nuclear Energy Agency, Issy-les-Moulineaux (France).
[6] S.B. Fisher, R.J. White, P.M.A. Cook, S. Bremier, R.C. Corcoran, R. Stratton, C.T. Walker, P.K. Ivison, I.D. Palmer, Microstructure of irradiated SBR MOX fuel and its relationship to fission gas release, J. Nucl. Mater. 306 (2–3) (2002) 153–172.
[7] P. Blair, J. Wright, The high burn-up disk irradiation test, IFA-655.1: results after three cycles of irradiation (HWR-776), Norway, 2004.
[8] A. Fernandez, J. McGinley, J. Somers, M. Walter, Overview of past and current activities on fuels for fast reactors at the institute for transuranium elements, J. Nucl. Mater. 392 (2) (2009) 133–138.
[9] A. Fernandez, K. Richter, J. Somers, Preparation of spinel (MgAl2O4) spheres by a hybrid sol-gel technique, CIMTECH-World ceramics congress and forum on new materials /World ceramics congress (Florence 1998-06-14), Techna, Faenza, 1999, pp. C167–C174.
[10] D.D. Sood, The role sol–gel process for nuclear fuels-an overview, J. Solgel. Sci. Technol. 59 (3) (2011) 404–416.
[11] J. Noirot, Y. Pontillon, S. Yagnik, J.A. Turnbull, T. Tverberg, Fission gas release behaviour of a 103GWd/tHM fuel disc during a 1200°C annealing test, J. Nucl. Mater. 446 (1) (2014) 163–171.
[12] J. Noirot, Y. Pontillon, S. Yagnik, J.A. Turnbull, Post-irradiation examinations and high-temperature tests on undoped large-grain UO2 discs, J. Nucl. Mater. 462 (2015) 77–84.
[13] T. Tverberg, The high burn-up disk irradiation test, IFA-655: final Report on the in-pile performance (HWR-837), 2008.
[14] M. Amaya, V. Grismanovs, T. Tverberg, Changes of the surface-to-volume ratio and diffusion coefficient of fission gas in fuel pellets during irradiation, J. Nucl. Mater. 402 (2) (2010) 108–115.
[15] P. Bennett, G. Rossiter, The High Burn-up disk irradiation test, IFA-655.1: results after the first cycle of irradiation, HWR-710 (2002).
[16] R.J. White, The fractal nature of the surface of uranium dioxide: a resolution of the short-lived/stable gas release dichotomy, J. Nucl. Mater. 295 (2) (2001) 133–148.
[17] R.J. White, J.A. Turnbull, A review of experiments, methodology and results from 1980 to 1997, Norway, 1998, p. 120.
[18] T. Tverberg, J. Wright, The high burn-up disk irradiation test, IFA-655: results after six cycles of irradiation (HWR-821), 2005.
[19] J.P. Hiernaut, T. Wiss, D. Papaioannou, R.J.M. Konings, V.V. Rondinella, Volatile fission product behaviour during thermal annealing of irradiated UO2 fuel oxidised up to U3O8, J. Nucl. Mater. 372 (2–3) (2008) 215–225.
[20] J.P. Hiernaut, P. Gotcu, J.Y. Colle, R.J.M. Konings, Thermodynamic study of actinides and lanthanides during total vaporisation of a very high burn-up UO2 fuel, J. Nucl. Mater. 378 (3) (2008) 349–357.
[21] J.-Y. Colle, E.A. Maugeri, C. Thiriet, Z. Talip, F. Capone, J.-P. Hiernaut, R.J.M. Konings, T. Wiss, A mass spectrometry method for quantitative and kinetic analysis of gas release from nuclear materials and its application to helium desorption from UO2 and fission gas release from irradiated fuel, J. Nucl. Sci. Technol. 51 (5) (2014) 700–711.
[22] T. Wiss, H. Thiele, A. Janssen, D. Papaioannou, V.V. Rondinella, R.J.M. Konings, Recent results of microstructural characterization of irradiated light water reactor fuels using scanning and transmission electron microscopy, J. Minerals Metals Mater. Soc. (TMS) 64 (12) (2012) 1390–1395.
[23] P. Pöml, S. Brémier, F. Lahuerte, R. Hasnoui, C.T. Walker, Calibration of a Cameca SX100 microprobe for the measurement of retained xenon in nuclear fuels, IOP Conf. Ser. Mater. Sci. Eng. 7 (1) (2010) 012025.
[24] M. Sheindlin, D. Halton, M. Musella, C. Ronchi, Advances in the use of laser-flash techniques for thermal diffusivity measurement, Rev. Sci. Instrum. 69 (3) (1998) 1426–1436.
[25] J.K. Fink, Thermophysical properties of uranium dioxide, J. Nucl. Mater. 279 (1) (2000) 1–18.
[26] H. Kleykamp, The chemical state of the fission products in oxide fuels, J. Nucl. Mater. 131 (2–3) (1985) 221–246.
[27] M. Rochedy, Thermochemical Behaviour of Corrosive Fission Products in Uranium Dioxide, University Paris Saclay, 2022.
[28] J. Magill, J. Galy, R. Dreher, D. Hamilton, M. Tufan, C. Normand, A. Schwenk–Ferrero, H.W. Wiese, NUCLEONICA: a nuclear science portal, Nucl. Data Sci. Technol., Proc. Int. Conf. (2007) 89–92.
[29] T. Wiss, V.V. Rondinella, R.J.M. Konings, D. Staicu, D. Papaioannou, S. Bremier, P. Pöml, O. Benes, J.-Y. Colle, P.V. Uffelen, A. Schubert, F. Cappia, M. Marchetti, D. Pizzocri, F. Jatuff, W. Goll, T. Sonoda, A. Sasahara, S. Kitajima, M. Kinoshita, Properties of the high burnup structure in nuclear light water reactor fuel, Radiochim. Acta 105 (11) (2017) 893–906.
[30] J.Y. Colle, J.P. Hiernaut, T. Wiss, O. Beneš, H. Thiele, D. Papaioannou, V.V. Rondinella, A. Sasahara, T. Sonoda, R.J.M. Konings, Fission product release and microstructure changes of irradiated MOX fuel at high temperatures, J. Nucl. Mater. 442 (1) (2013) 330–340.
[31] J. Spino, J. Rest, W. Goll, C.T. Walker, Matrix swelling rate and cavity volume balance of UO2 fuels at high burn-up, J. Nucl. Mater. 346 (2) (2005) 131–144.
[32] C. Ronchi, M. Sheindlin, D. Staicu, M. Kinoshita, Effect of burn-up on the thermal conductivity of uranium dioxide up to 100.000 MWdt−1, J. Nucl. Mater. 327 (1) (2004) 58–76.
[33] W. Wiesenack, Assessment of UO2 conductivity degradation based on in-pile temperature data, Proc. Int. Topical Mtg. on LWR Fuel Perf. (1997) 507–515 ANS, Portland, Oregon.
[34] L. Desgranges, C. Valot, B. Pasquet, J. Lamontagne, T. Blay, I. Roure, A method for the quantification of total xenon concentration in irradiated nuclear fuel with SIMS and EPMA, Nucl. Instrum. Methods Phys. Res. Sect. B 266 (1) (2008) 147–154.
[35] W.J. Weber, R.C. Ewing, E.R. Vance, D. Gregg, S. Peuget, T. Wiss, Plutonium in Waste Forms, 2nd ed., Plutonium Handbook, 2019 ed..
[36] R.J.M. Konings, T. Wiss, O. Beneš, Predicting material release during a nuclear reactor accident, Nat. Mater. 14 (3) (2015) 247–252.
[37] J.P. Hiernaut, T. Wiss, J.Y. Colle, H. Thiele, C.T. Walker, W. Goll, J.R.M. Konings, Fission product release and microstrucrure changes during laboratory annealing of a very high burn-up fuel specimen, J. Nucl. Mater. 377 (2) (2008) 313–324.
[38] M. Pelletier, Y. Guérin, 2.03 Fuel Performance of Fast Spectrum Oxide Fuel, in: R.J.M. Konings, R.E. Stoller (Eds.), Comprehensive Nuclear Materials, Elsevier, Oxford, 2020, pp. 72–105.
[39] R.A. Clark, M.A. Conroy, T.G. Lach, E.C. Buck, K.L. Pellegrini, B.K. McNamara, J.M. Schwantes, Distribution of metallic fission-product particles in the cladding liner of spent nuclear fuel, NPJ Mater Degrad. 4 (1) (2020) 4.